Scaling of the turbulent/non-turbulent interface in boundary layers

Kapil Chauhan†, Jimmy Philip and Ivan Marusic

Department of Mechanical Engineering, The University of Melbourne, Parkville, VIC 3010, Australia

Scaling of the interface that demarcates a turbulent boundary layer from the non-turbulent free stream is sought using theoretical reasoning and experimental evidence in a zero-pressure-gradient boundary layer. The data-analysis, utilising particle image velocimetry (PIV) measurements at four different Reynolds numbers ($\delta u_\tau / \nu = 1200$–$14\,500$), indicates the presence of a viscosity dominated interface at all Reynolds numbers. It is found that the mean normal velocity across the interface and the tangential velocity jump scale with the skin-friction velocity u_τ and are approximately $u_\tau / 10$ and u_τ, respectively. The width of the superlayer is characterised by the local vorticity thickness δ_ω and scales with the viscous length scale ν / u_τ. An order of magnitude analysis of the tangential momentum balance within the superlayer suggests that the turbulent motions also scale with inner velocity and length scales u_τ and ν / u_τ, respectively. The influence of the wall on the dynamics in the superlayer is considered via Townsend's similarity hypothesis, which can be extended to account for the viscous influence at the turbulent/non-turbulent interface. Similar to a turbulent far-wake the turbulent motions in the superlayer are of the same order as the mean velocity deficit, which lends to a physical explanation for the emergence of the wake profile in the outer part of the boundary layer.

Key words: boundary-layer structure, boundary layers, turbulent boundary layers, turbulent flows

---

1. Introduction

All turbulent flows and their different turbulence characteristics are affected by the boundaries within which they reside. These boundaries are rigid, flexible, fluid or a combination thereof. Substantial research has been devoted to the case where a flow is bounded by a rigid surface with prominent emphasis on near-wall dynamics, e.g. duct flows, turbulent boundary layers, impinging jets, wall-jets, etc. The case where a turbulent flow has a fluid boundary is relatively more complex, e.g. combustion flame fronts, mixing of non-identical fluids, turbulent flow bounded by a non-turbulent flow, etc. Here we focus on the boundary between the turbulent and non-turbulent flow in canonical zero-pressure-gradient turbulent boundary layers.

In practice, the turbulent/non-turbulent interface (TNTI) is detected in many different ways such as hot-wire signal (skewness, variance, gradients), scalar

† Email address for correspondence: kchauhan@unimelb.edu.au

concentration, vorticity, etc. Using vorticity as a criterion to demarcate turbulent/non-turbulent regions, da Silva & Taveira (2013) have shown the existence of a region where the diffusion of enstrophy is dominant while its production is negligible, the region suggested to be the viscous superlayer in accordance with the description of Corrsin & Kistler (1955). In the immediate vicinity of this region (towards the turbulent side) is the region where the peak in vorticity occurs and is defined as the '*turbulent sublayer*' (da Silva *et al.* 2014). The interface layer is suggested to have these two layers. The results of da Silva & Taveira (2013) are obtained using a vorticity criteria to identify the TNTI in a turbulent jet. It remains to be seen whether their observations apply to other flows, especially at high Reynolds numbers and for different TNTI detection criteria.

Until recently, for the majority of studies, the limited resolution of probing techniques have been able to identify the region with vorticity concentration (the thickness of this region is found to be of the order of λ_T, the Taylor microscale in shear flows), while the existence of a region with dominant viscous diffusion was only hypothesised. This is due to the fact that the thickness of the viscous diffusion region is small and of the order of the Kolmogorov scale. (Based on dimensional arguments Corrsin & Kistler (1955) estimate the thickness to be of the order of $\sqrt{\nu/\omega}$, where ν is the kinematic viscosity and ω is the vorticity magnitude.) Using direct numerical simulations, da Silva & Taveira (2013) specify that one would require a fine resolution (grid spacing no larger than η, the Kolmogorov scale) to detect this region. The experimental database used in the present study lacks the resolution to identify the region where diffusion is prominent. However, the limited interrogation size does allow us to identify the region with vorticity peak (as will be shown in § 3.3). Furthermore, it is noted that various approaches that can be used to identify TNTI are consistent and reveal similar overall characteristics (Anand, Boersma & Agrawal 2009; de Silva *et al.* 2013; Chauhan *et al.* 2014). In our study we have utilised a kinetic energy (KE) criteria to identify the TNTI, particularly, as we only have access to one component of vorticity and not the full enstrophy. Chauhan *et al.* (2014) described in detail the KE criteria and established the appropriateness of using the KE criteria to identify the TNTI. Although it is not certain whether the KE criteria can identify a subregion where vorticity diffusion occurs, Taveira & da Silva (2013) have shown that the conditional KE profile exhibits a sharp rise at the interface where the TNTI is identified by a vorticity criteria. If two such regions are identifiable with a KE criteria, we acknowledge that the limited resolution of data presented here fails to reveal the diffusion layer. Since the thickness of the vorticity/enstrophy concentration region is much larger than the thickness over which diffusion occurs, we follow the common convention to collectively refer to these two regions as the superlayer. Therefore, in this paper we use the term 'superlayer' to refer to the region with vorticity concentration that is identified with the KE criterion.

The scaling of the TNTI in turbulent boundary layers can be pursued in two complimentary aspects; global as well as local. The *global* aspect is related to the mean growth rate of the turbulence boundary, its organisation and entrainment. Globally different flows behave differently, especially shear-free and shear flows, with further differences among the various shear flows (Philip & Marusic 2012). However, it is in the local aspects where there is a hope of universality (Sreenivasan, Ramshankar & Meneveau 1989*b*). Philip *et al.* (2014) utilise a multi-scale analysis to show that entrainment from global and local views can be considered as viewing the flow from different scales. They examined molecular diffusion of KE and viscous nibbling at the smallest scale, focussing on correlations between interface orientation,

viscous stress tensor elements, and local fluid velocity. At the largest scale, the total KE is shown to evolve predominantly due to the turbulent advective fluxes occurring through an average surface which differs considerably from the local, corrugated, sharp interface.

The emphasis of the current study is the local aspect that pertains to the conditionally averaged velocity and variance profiles, as well as the velocity and length scale characteristics of and within the interface, utilising data spanning more than a decade in Reynolds number. Developments in characterising these features are fairly nascent and made possible by the recent advances in experimental techniques and numerical methods. Holzner & Lüthi (2011) have shown that the interface thickness scales with the Kolmogorov scale in a TNTI under a shear-free flow. On the other hand, the thickness of the interface layer is found to be of the order of the Taylor microscale (λ_T) in flows with mean shear (e.g. Bisset, Hunt & Rogers 2002 in wakes, da Silva & Taveira 2010 in jets). Furthermore, da Silva & dos Reis (2011) have shown that in flows with mean shear the presence of vortical structures at the interface, the radius of which is $O(\lambda_T)$, determine the thickness of the layer, while in flows without mean shear the thickness scales with the Kolmogorov scale. Pertaining to the length scales of turbulent motions responsible for entrainment, Holzner et al. (2007) have shown that they are essentially small scales in shear-free flow, and evidenced to be of the order of Taylor microscale by Westerweel et al. (2005) and da Silva & Pereira (2008). Similar observation in a zero-pressure-gradient turbulent boundary layer at high Reynolds number ($\delta^+ = \delta u_\tau/\nu \approx 14\,500$, where $u_\tau = \sqrt{\tau_w/\rho}$ is the skin-friction velocity) is made by Chauhan et al. (2014), wherein autocorrelation of the normal velocity at the interface and instantaneous mass-flux analysis indicate that motions of $O(\lambda_T)$ are representative of small-scale features. Further, by means of 'mass-flux spectra' it is shown that the boundary layer entrainment is characterised by two distinctive length scales ($O(\lambda_T)$ and $O(\delta)$) with a large separation between them with increasing Reynolds number.

The local entrainment velocity (v_n, normal velocity relative to the interface) is found to scale with the Kolmogorov velocity (v_K) in a TNTI emerging from an oscillating grid (shear-free flow) by Holzner & Lüthi (2011). The local entrainment velocity depends significantly on the surface shape of the interface as evidenced by Wolf et al. (2012, 2013) in a turbulent jet flow. For turbulent boundary layers v_n scales with u_τ (Philip et al. 2014). On the other hand, the mean propagation velocity of the interface can be obtained from the growth rate of the mean turbulence boundary ($d\delta/dx$ in boundary layers and db/dx in jets/wakes, where b is the half-width). The mean entrainment velocity relative to the interface can then be calculated from the average mass-flux in the flow, e.g. for the case of an axisymmetric jet, $E = -E_b/2$, where E_b is the rate at which the turbulent flow is spreading and E is the rate at which external fluid flows into the turbulent flow across the interface (Turner 1986). In the present paper an analogous expression (3.4) for the mean entrainment velocity is verified for boundary layers under zero pressure gradient.

As indicated above, recent studies have focussed primarily on the shear-free (oscillating grid) and free-shear (jets/wakes) flows, while the case of a turbulent boundary layer (wall-bounded shear flow) has received less attention, even though it is also of much practical importance. For boundary-layer flows, two distinct length scales (inner, ν/u_τ, and outer, δ) are required to characterise the mean-flow similarity. It is also known that in the outer region (considered as the logarithmic layer and beyond) the turbulent motions of the order of δ influence the dynamics in the logarithmic region and below (Hutchins & Marusic 2007). The TNTI, wherein viscous effects are
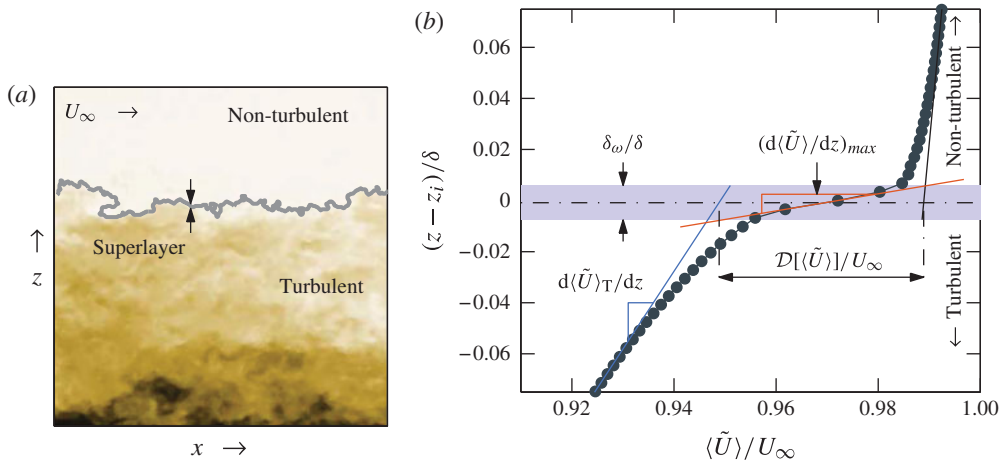
FIGURE 1. (Colour online) (*a*) Example of an instantaneous TNTI (grey line) shown over contours of total streamwise velocity. (*b*) Conditionally averaged streamwise velocity with respect to the interface position z_i for $\delta^+ = 14\,500$. The line —•— shows $\langle \tilde{U} \rangle / U_\infty$; solid lines indicate local slopes. The shaded region is equivalent to the vorticity thickness δ_ω and is indicative of the superlayer width.

dominant, resides in the intermittent region of the boundary layer ($z/\delta \gtrsim 1/3$); the interaction is between the small scales (that carry the viscous influence) and the large scales (that are predominantly inviscid). In this paper we focus on the small-scale aspects by examining the superlayer at four distinct Reynolds numbers. To this end we concentrate on scaling of the mean thickness, streamwise velocity jump and mean entrainment velocity by examining different *Re* zero-pressure-gradient flows.

For future reference we note that, in the laboratory frame of reference, the streamwise and wall-normal axes are represented by x and z. The instantaneous streamwise velocity, wall-normal velocity and spanwise vorticity are represented by $\tilde{U}$, $\tilde{W}$ and $\tilde{\Omega}_y$, respectively. The corresponding mean quantities are denoted as U, W and Ω_y and lowercase symbols are used for fluctuating components (u, w and ω_y), e.g. $\tilde{U} = U + u$. The superscript '+' indicates the scaling by inner velocity (u_τ) and length (ν/u_τ). The subscript 'i' denotes quantities at the interface. The conditional averages over the interface are indicated by $\langle \ \rangle$, while the fluctuating quantities with respect to the conditional mean are denoted as lowercase symbols with '$\prime$' superscript (u', w' and ω_y'), e.g. $\tilde{U} = \langle \tilde{U} \rangle + u'$.

1.1. *Problem definition*

Consider figure 1 which shows the conditionally averaged streamwise velocity profile with reference to the local interface position z_i for $Re_\tau = 14\,500$ (Chauhan *et al.* 2014). The average profile is obtained as one moves along the interface and profiles for instantaneous quantities are collected over the ordinate $z - z_i$ for subsequent averaging. As one crosses the interface from the turbulent region to the non-turbulent region a steep rise in $\langle \tilde{U} \rangle$ is observed accompanied by corresponding change in the wall-normal gradient. The steep rise occurs in a narrow region which is the superlayer. If the linear gradients in the turbulent and non-turbulent regions are extrapolated, we see that a jump in velocity across the superlayer has to occur at $z - z_i = 0$. This jump is denoted

as $\mathcal{D}[\langle \tilde{U} \rangle]$. Thereby, the measured jump in $\langle \tilde{U} \rangle$ and the maxima of its local gradient aids in defining the vorticity thickness (e.g. Brown & Roshko 1974).

$$\delta_\omega \equiv \frac{\mathcal{D}[\langle \tilde{U} \rangle]}{\left. \dfrac{\mathrm{d}\langle \tilde{U} \rangle}{\mathrm{d}z} \right|_{max}}. \tag{1.1}$$

Chauhan *et al.* (2014) have shown that the vorticity thickness is an appropriate measure of the width of the superlayer by spectra of the instantaneous mass-flux across the interface that the length scales involved in the small-scale nibbling mechanism are of the same order as the vorticity thickness. Nibbling refers to the propagation of vorticity from the turbulent region into the non-turbulent region by viscous diffusion through small-scale eddy motions in the vicinity of the TNTI. The questions that then emerge with respect to the scaling with varying Reynolds numbers are as follows.

(*a*) What can one say about the mean entrainment velocities at the interface?

(*b*) How does the jump in $\langle \tilde{U} \rangle$ and the vorticity thickness, δ_ω, vary with Re_τ?

(*c*) What is the scale of turbulent velocity fluctuations within the superlayer?

Answering the above questions is the main aim of this study and they are addressed in § 3. Starting with the experimental evidence in § 3.1, velocity scales for the mean flow (relative to the interface) are first established. Thereafter the governing equations that are relevant to the superlayer dynamics is outlined in § 3.2 and an order of magnitude analysis is undertaken. The conclusions made for scaling from the order of magnitude analysis are attested with results from experiments in § 3.3. Subsequent discussion on the emergence and implications of the observed scaling is presented in § 4, followed by the summary in § 5.

2. Experimental database

The present study utilises particle image velocimetry (PIV) data. Two-dimensional velocity fields in the streamwise/wall-normal plane at four different Reynolds numbers over a range $\delta^+ = 1200$–$14\,500$ are considered. Previous PIV experiments contribute to the present data and the key experimental parameters are summarised in table 1. The present data (data sets C and D in table 1) are from the high-Reynolds-number boundary layer wind tunnel (HRNBLWT) at the University of Melbourne. The experiments listed in table 1 were performed under nominally zero streamwise pressure-gradient conditions. The streamwise pressure-gradient is within $\pm 0.5\,\%$ and $\pm 2\,\%$ of the freestream velocity for HRNBLWT and Adrian *et al.* (2000), respectively. The freestream turbulence intensity ($\overline{uu}^{1/2}/U_\infty$) is less than 0.2 %, 0.5 % and 0.2 % of the freestream velocity for the data of Adrian *et al.* (2000), Hambleton *et al.* (2005) and HRNBLWT (Kulandaivelu 2012), respectively. Further details of each measurement can be found in the corresponding references. The boundary-layer thickness δ for the Adrian *et al.* (2000) and Hambleton *et al.* (2005) profiles is re-evaluated here by a fit to the composite velocity profile of Chauhan, Monkewitz & Nagib (2009) for consistency. The TNTI in these velocity fields is detected using a KE criteria, where the threshold $\tilde{k}$ for each flow is established using the procedure outlined by Chauhan *et al.* (2014) in order to obtain a good agreement of the intermittency profile with other data in the form of an error function. The local

Experiment	δ^+	U_∞ (m s^{-1})	δ (m)	u_τ (m s^{-1})	$L_x \times L_z$	$\Delta x^+ \times \Delta z^+$	% overlap	$\tilde{k}$	N_f	Symbol
A	1230	6	0.08	0.25	$1.5\delta \times 1.34\delta$	32×32	50	0.15	1478	◆
B	2790	11.4	0.1	0.41	$1.4\delta \times 1.4\delta$	36×25	50	0.15	50	▶
C	7870	10	0.36	0.33	$2\delta \times 1.1\delta$	52×52	50	0.12	1190	●
D	14 500	20	0.35	0.63	$2\delta \times 1.1\delta$	49×49	50	0.12	1250	■

TABLE 1. Experimental parameters of the four data sets analysed: A, Hambleton, Hutchins & Marusic (2005); B, Adrian, Meinhart & Tomkins (2000); C, D, present study. Here $L_x \times L_z$ is the field of view in the streamwise/wall-normal plane and $\Delta x^+ \times \Delta z^+$ is the corresponding vector spacing. We use $\tilde{k}$ to denote the threshold on local turbulent KE to distinguish the turbulent from the non-turbulent regions in the approach of de Silva *et al.* (2013) and Chauhan *et al.* (2014). Here N_f is the number of frames of vector fields. The experimental set-up and procedures for the present study are elaborated in de Silva *et al.* (2012), Chauhan *et al.* (2014) and de Silva *et al.* (2014).

turbulent KE in the frame of reference moving with U_∞, over a 3×3 grid is defined as

$$\tilde{k} = 100 \times \frac{1}{9\,U_\infty^2} \sum_{m,n=-1}^{1} [(\tilde{U}_{m,n} - U_\infty)^2 + (\tilde{W}_{m,n})^2]. \tag{2.1}$$

The above definition is suitable to distinguish between the turbulent regions where the KE of fluctuations is high from the non-turbulent regions where the KE of fluctuations is nearly zero. A detailed discussion on the KE criteria is found in Chauhan *et al.* (2014). The consistency of using a KE criteria is evident in the recent results of de Silva *et al.* (2013) and Chauhan *et al.* (2014). We note that the present data is limited to two dimensions in the wall-normal–streamwise plane. Even though in the mean equation all terms that are present can be evaluated from this 2D measurement (which is carried out here), a fuller investigation of interface characteristics will be aided by 3D data, which unfortunately is not accessible in the present experimental set-up with a large field of view at these high *Re*.

Before proceeding further, we give a note on the measurement resolution in these studies. For the four different *Re* boundary layers examined here, the ratio of the interrogation window size (Δ_i) to the Kolmogorov scale varies between 4 and 6 in the outer region. This finite window size has a filtering effect and thus motions that are smaller than the window size cannot be resolved. Obviously this limits us from isolating a region at the TNTI where viscous diffusion is prominent, since this region can only be resolved with a grid spacing smaller than the Kolmogorov scale according to da Silva *et al.* (2014). Even so, the large dynamic range obtained in these experiments ($L_x/\Delta x$ or $L_z/\Delta z$, see table 1) justifies the compromise made in not resolving scales that are approximately of size η. On the other hand, the ratio of the Taylor microscale to the interrogation window size approximately ranges from 2 to 3. The overall layer thickness (dictated by the region of vorticity peak) is of the order of the Taylor microscale in flows with mean-shear (da Silva & dos Reis 2011). Therefore, it is possible to identify this layer of vorticity concentration (as will be shown in § 3.3) in these data sets. (See (4.3) for the definition of Kolmogorov length scale and Taylor microscale.)

3. Analysis

3.1. *Mean velocity scales (relative to the interface)*

The mean interface location, Z_i, when normalised by the local boundary-layer thickness is Reynolds number independent, i.e. $Z_i/\delta \approx 2/3$. Owing to this property we consider the developing boundary layer as either of the two configurations shown in figure 2(*a,b*). Figure 2(*a*) is the typical boundary-layer schematic where the turbulent flow resides within the thickness δ, while the mean velocity profile gradually approaches the free-stream velocity. The mean entrainment into the layer can be determined from the free-stream velocities U_∞ and W_∞ at the layer's edge. In the alternate average schematic of figure 2(*b*) it is considered that the turbulent flow is confined below the superlayer at $Z_i = 2\delta/3$. The flow above the superlayer is non-turbulent and the streamwise velocity undergoes a sudden change within the superlayer. In this case the mean entrainment is determined by the mean velocities at the interface, i.e. $\langle \tilde{U}_i \rangle$ and $\langle \tilde{W}_i \rangle$ in the streamwise and wall-normal directions, respectively. Using experimental data at $\delta^+ = 14\,500$, Chauhan *et al.* (2014) showed
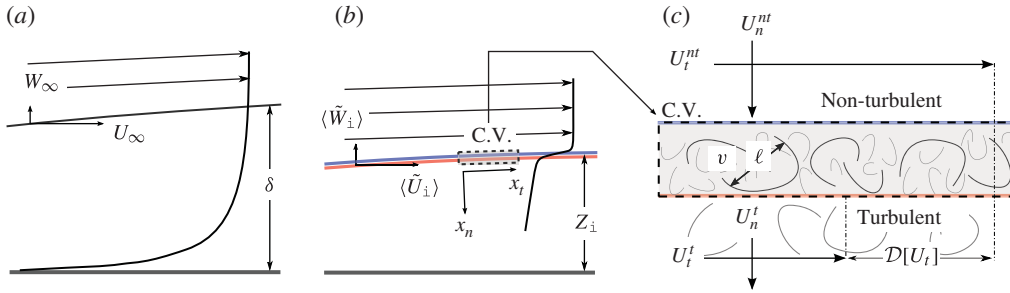
FIGURE 2. (Colour online) Two average schematics. (*a*) Schematic of the mean boundary layer, where U_∞ and W_∞ are the free-stream velocities in the streamwise and wall-normal directions, respectively, and δ is the boundary layer thickness. (*b*) Schematic of a turbulent flow below a mean interface. 'C.V.' denotes the control volume. Here $\langle \tilde{U}_i \rangle$ and $\langle \tilde{W}_i \rangle$ are averaged streamwise and wall-normal velocities respectively, conditioned at the interface and Z_i is the mean interface height. Subscripts '*n*' and '*t*' denote normal and tangential directions, respectively. (*c*) Control volume along the superlayer. Superscripts '*nt*' and '*t*' denote non-turbulent and turbulent regions, respectively, and v and ℓ are characteristic velocity and length, respectively, of turbulent motions within the superlayer.

Experiment	δ^+	Left-hand side	Right-hand side
A Hambleton *et al.* (2005)	1230	0.10	0.08
B Adrian *et al.* (2000)	2790	0.13	0.13
C Present study	7870	0.11	0.11
D Present study	14 500	0.21	0.22

TABLE 2. Net entrainment $d\dot{m}/dx$ calculated from the left-hand side and right-hand side of (3.1).

that the entrainment calculations using either of the above approaches are consistent and result in the equation

$$\frac{d\dot{m}}{dx} = U_\infty \left[\frac{d\delta}{dx} - \frac{d\delta^*}{dx} \right] \approx \left[\langle \tilde{U}_i \rangle \frac{Z_i}{\delta} \frac{d\delta}{dx} - \langle \tilde{W}_i \rangle \right]. \tag{3.1}$$

Here δ^* is the displacement thickness. The above equation is validated for the four data sets by estimating the net mass flux $d\dot{m}/dx$ using both sides of the equation. The resulting values for $d\dot{m}/dx$ from the theory (left-hand side of (3.1)) are compared with those obtained from conditional mean velocities at the interface (right-hand side of (3.1)) in table 2 and found to be in good agreement.

Now, the ratio Z_i/δ is less than one and approximately equal to 2/3. The outer similarity of the mean flow at high Reynolds numbers implies that $\langle \tilde{U}_i \rangle / U_\infty \sim 1$. Using the expressions for $d\delta/dx$ and $d\delta^*/dx$ (see appendix A in Chauhan *et al.* 2014, or other equivalent evolution equations) we get

$$\frac{\langle \tilde{W}_i \rangle}{U_\infty} \approx \underbrace{\frac{1}{(U_\infty^+)^2} \left[\frac{H\kappa}{H I_{WW}/(U_\infty^+)^2 + \kappa} \right]}_{= d\delta^*/dx} - \frac{1}{3} \frac{\delta^+}{Re_{\delta^*}} \frac{1}{U_\infty^+} \underbrace{\left[\frac{H(\kappa + 1/U_\infty^+)}{H I_{WW}/(U_\infty^+)^2 + \kappa} \right]}_{= d\delta/dx}, \tag{3.2}$$

where κ is the von Kármán's constant, $H = \delta^*/\theta$ is the shape factor, θ is the displacement thickness, $I_{WW} = \int_0^\infty (U_\infty^+ - U^+)^2 \mathrm{d}(z/\Delta)$ with $\Delta = U_\infty \delta^*/u_\tau$ and $Re_{\delta^*} = U_\infty \delta^*/\nu$. Since $Re_{\delta^*}/\delta^+ \approx 3.4$ at high Reynolds numbers (Chauhan *et al.* 2009), the second term on the right is U_∞^+ times larger than the first term on the right. Therefore

$$\frac{\langle \tilde{W}_i \rangle}{U_\infty} \approx -\frac{1}{3}\frac{\mathrm{d}\delta}{\mathrm{d}x}. \tag{3.3}$$

Since $E_b = U_\infty \mathrm{d}\delta/\mathrm{d}x$, the mean spreading velocity of the boundary layer. Therefore

$$\langle \tilde{W}_i \rangle \approx -\frac{E_b}{3}. \tag{3.4}$$

In the experiments analysed here the boundary layer is examined in the Eulerian frame of reference and under a fixed free-stream velocity the boundary layer thickness remains unchanged. Since the location of the mean interface also does not change, the mean propagation velocity of the interface at a fixed position in x is zero. This implies that the measured conditional velocity ($\langle \tilde{W}_i \rangle$) at the interface is then the mean entrainment velocity across the interface. Therefore (3.4) is an approximate expression that relates the mean entrainment velocity to the growth of the layer, analogous to a similar expression by Turner (1986) for turbulent jets. Furthermore, the shape factor $H \to 1$ (Monkewitz, Chauhan & Nagib 2008) in the limit $U_\infty^+ \to \infty$ for a zero-pressure-gradient boundary layer (for example, at $\delta^+ = 14\,500$, $Re_{\delta^*}/\delta^+ \approx 3.6$, $H \approx 1.3$ and $\mathrm{d}\delta/\mathrm{d}x \approx 0.012$ which correspond to a slow boundary layer growth of approximately $0.7°$). Equation (3.2) then simplifies to

$$\frac{\langle \tilde{W}_i \rangle}{u_\tau} \approx -\frac{1}{10}. \tag{3.5}$$

The constraint of (3.1) in the developing boundary layer establishes that $\langle \tilde{W}_i \rangle$ is proportional to u_τ, i.e. $\langle \tilde{W}_i \rangle \sim u_\tau$. Equation (3.5) is an approximate expression for the mean entrainment velocity. It is noted that $\langle \tilde{W}_i \rangle$ at the interface is negative, which is consistent with the notion that the mean influx of momentum is from the non-turbulent region to the turbulent region, in contrast to positive W_∞. Figure 3(*a*) shows profiles of $\langle \tilde{W} \rangle / u_\tau$ from PIV measurements for the four Reynolds numbers. Hereafter the wall-normal distance from the interface is denoted as $\xi = z - z_i$. A good agreement of the profiles is seen over the wide range of Reynolds numbers on the non-turbulent side. On the turbulent side the profile for Adrian *et al.* (2000) deviates from the rest, however, a lack of Reynolds number trend in this region is evident. For the Adrian *et al.* (2000) data set, the number vector fields were considerably small ($N_f = 50$) which likely makes it difficult to obtain converged results especially for the wall-normal component that is at least two orders of magnitude smaller than the streamwise component. It is also seen that in the vicinity of the detected interface location and above it, i.e. $\xi \gtrsim 0$, the average wall-normal velocity is negative and in good agreement with the approximation of (3.5).

A note on the dynamic range of the measurements in turbulent boundary layers is warranted here especially for the wall-normal component. The average wall-normal velocity is approximately two orders of magnitude smaller than the average streamwise velocity in a turbulent boundary layer. For PIV measurements this characteristic implies that the displacement of the interrogation region in the wall-normal direction
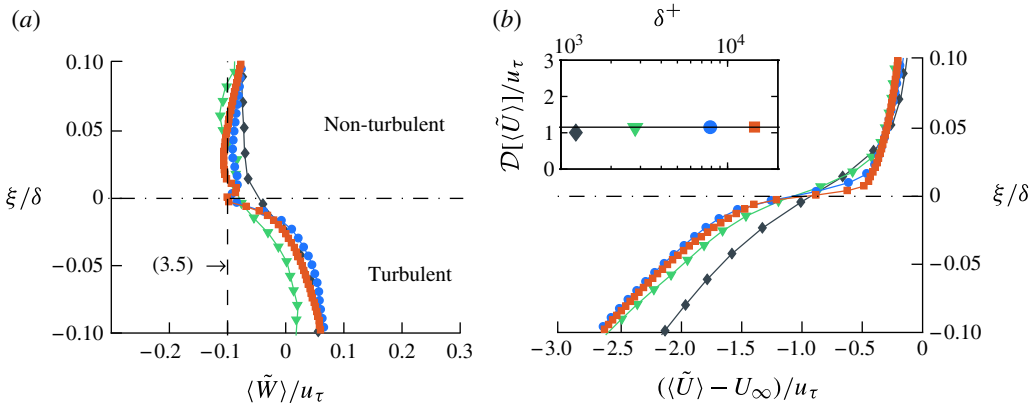
FIGURE 3. (Colour online) Conditionally averaged velocities with respect to the interface position z_i. (*a*) Wall-normal velocity, $\langle \tilde{W} \rangle$. Dashed vertical line is (3.5). (*b*) Streamwise velocity, $\langle \tilde{U} \rangle$. Symbols indicate: (black) —◆—, $\delta^+ = 1230$ (Hambleton *et al.* 2005); (green online) —▼—, $\delta^+ = 2790$ (Adrian *et al.* 2000); (blue online) —●—, $\delta^+ = 7870$; (red online) —■—, $\delta^+ = 14\,500$. The inset in (*b*) shows variation of $\mathcal{D}[\langle \tilde{U} \rangle]/u_\tau$ with δ^+.

is less than one pixel and typically in the range 0.25–0.5 pixels. Hence the resolved wall-normal velocity is susceptible to bias errors due to peak-locking (Christensen 2004). The extent of this bias error is dependent on the accuracy of the subpixel displacement estimator (such as the Gaussian estimator adopted in our study) that typically is 0.1 pixels. Therefore, caution needs to be exercised in examining the distribution of $\langle W \rangle$, which is only few times our measurement accuracy.

Equivalence of the mean entrainment rates calculated for cases (*a*) and (*b*) of figure 2 implies that the bulk flow within each layer is the same. For the conventional boundary-layer schematic in figure 2(*a*) the bulk flow velocity U_b with the boundary layer is given as

$$U_b = \int_0^1 U \, d(z/\delta) = U_\infty \int_0^1 1 - \left(1 - \frac{U}{U_\infty}\right) d(z/\delta) = U_\infty \left(1 - \frac{\delta^*}{\delta}\right). \qquad (3.6)$$

Utilising the defect form and knowing that the ratio Δ/δ asymptotes to a constant with increasing *Re*, we get

$$\frac{U_\infty - U_b}{u_\tau} \approx \frac{U_\infty}{u_\tau} \frac{\delta^*}{\delta} = \frac{\Delta}{\delta} \to 3.4. \qquad (3.7)$$

The above equation implies that the defect of the bulk velocity in the turbulent boundary layer scales with u_τ at high Reynolds numbers. The above equation is not surprising and merely an implication of the outer mean flow similarity in zero-pressure-gradient turbulent boundary layers, i.e.

$$\frac{U - U_\infty}{u_\tau} = f_o(z/\delta), \quad z/\delta \to 1. \qquad (3.8)$$

Here $f_o(z/\delta)$ is the outer similarity profile for the mean flow that is independent of Reynolds number and valid in and above the overlap region. In figure 1 the

conditional streamwise velocity is built across the interface that is known to reside in the intermittent region ($\delta/3 \lesssim z_i \lesssim \delta$). Since the conditional profile is obtained by averaging from a region in which the streamwise velocity deficit scales with u_τ (3.8), we can expect the deficit of the conditionally averaged streamwise velocity to also scale with u_τ. Therefore the conditionally averaged streamwise velocity profiles from the four Reynolds number data sets available to us are plotted in figure 3(*b*) in the defect form and normalised by u_τ, i.e. ($\langle \tilde{U} \rangle - U_\infty)/u_\tau$. The profiles exhibit a Reynolds number trend for $\langle \tilde{U} \rangle^+ - U_\infty^+$ mostly in the region $-0.01 \lesssim \xi/\delta \lesssim 0.05$. In the turbulent and non-turbulent regions excluding this region an agreeable collapse of profiles is observed. On the turbulent side ($\xi/\delta < 0$), the lowest *Re* profile of Hambleton *et al.* (2005) deviates from the rest, however a lack of trend in the remaining profiles is suggestive of *Re*-independence at higher Reynolds numbers. A sharp rise in ($\langle \tilde{U} \rangle - U_\infty)/u_\tau$ for all profiles is seen as one moves from the turbulent region to the non-turbulent region. This characteristic is indicative of the presence of a superlayer in all four data sets examined in this study. Similar to figure 1, the linear trends of ($\langle \tilde{U} \rangle - U_\infty)/u_\tau$ in the turbulent and non-turbulent regions are extrapolated for all profiles to determine the jump $\mathcal{D}[\langle \tilde{U} \rangle]/u_\tau$ that would appear at $\xi = 0$. The resulting $\mathcal{D}[\langle \tilde{U} \rangle]/u_\tau$ are plotted versus δ^+ in the insert of figure 3(*b*). A convincing agreement in the form of Reynolds number independence is found for $\mathcal{D}[\langle \tilde{U} \rangle]/u_\tau$ over a range of $\delta^+ = 1200$–$14\,500$. The agreement implies that the jump across the superlayer scales with the skin-friction velocity u_τ irrespective of the free-stream velocity. It is found that

$$\frac{\mathcal{D}[\langle \tilde{U} \rangle]}{u_\tau} \approx 1.15 \Rightarrow \mathcal{D}[\langle \tilde{U} \rangle] \sim u_\tau. \tag{3.9}$$

If one considers the entrainment hypothesis set by Morton, Taylor & Turner (1956) that the local rate of entrainment is proportional to some characteristic velocity, we find in our study that indeed the mean entrainment velocity (3.5) is proportional to u_τ. The characteristic velocity is usually the local time-averaged mean velocity and in the case of the boundary layer is proportional to the difference between the mean velocity inside and outside the turbulent region (Hunt, Rottman & Britter 1984; Turner 1986). Similarity of the mean velocity deficit ($U - U_\infty$) when normalised by u_τ in the outer region of a zero-pressure-gradient turbulent boundary layer is well-known (3.8). Considering $U(z/\delta) - U_\infty$ as the characteristic velocity at a particular z/δ, the local entrainment velocity will be proportional to this deficit according to the entrainment hypothesis. Since $(U(z/\delta) - U_\infty)/u_\tau = O(1)$ in the intermittent region, on average, the skin-friction velocity u_τ is then appropriate to characterise the mean entrainment. This conclusion is consistent with (3.5) obtained in the present study which is derived based on the mean growth of the boundary layer. Thus, (3.5) not only agrees well with the data (figure 1*a*) but also adheres to the entrainment hypothesis of Morton *et al.* (1956).

3.2. *The governing equations*

The emphasis in this subsection is on a thin control volume along the superlayer as illustrated in figure 2(*b*) (dashed box). The control volume is shown in detail in figure 2(*c*). Following Reynolds (1972), an orthogonal coordinate system can be defined with n, t and p axes that has its local origin at the interface. The perpendicular to n–t plane is positive going into the plane of the paper. The mean velocity in the

p direction is zero by the assumption of homogeneity. The mean tangential and normal velocities on the non-turbulent side of the control volume are denoted as U_t^{nt} and U_n^{nt}, respectively, and similarly the velocities on the turbulent side are denoted as U_t^t and U_n^t. Fluctuating components are u_t' and u_n' in the tangential and normal direction, respectively. Across the control volume, i.e. the superlayer, a sharp change in tangential velocity occurs such that $U_t^{nt} \neq U_t^t$. The difference in U_t^{nt} and U_t^t is denoted using the difference operator $\mathcal{D}$, i.e. $\mathcal{D}[U_t] = U_t^{nt} - U_t^t$. Homogeneity in the tangential and perpendicular directions is assumed, i.e. $\partial(\ )/\partial x_t = 0$ and $\partial(\ )/\partial x_p = 0$ for averaged quantities. From the continuity equation,

$$\frac{\partial U_n}{\partial x_n} = 0 \Rightarrow U_n^{nt} = U_n^t. \tag{3.10}$$

Equation (3.10) is the same as the first of four superlayer jump conditions obtained by Reynolds (1972). Now the turbulent boundary layer under a zero pressure gradient grows gradually and the growth rate decreases further downstream ($d\delta/dx \to 0$). Although the instantaneous interface is contorted, the average interface is bounded by the slow growth rate of the boundary layer itself, i.e. $dZ_i/dx \approx (Z_i/\delta) \cdot (d\delta/dx)$ (Chauhan *et al.* 2014). Under such conditions the wall-normal velocity $\tilde{W}$ will contribute the most to the velocity normal to the mean interface while the streamwise velocity $\tilde{U}$ will dominate the mean tangential velocity. Therefore, one can make the approximations

$$\mathcal{D}[U_t] \approx \mathcal{D}[\langle \tilde{U} \rangle] \sim u_\tau, \tag{3.11}$$

and

$$U_n^{nt} = U_n^t \approx -\langle \tilde{W}_i \rangle \sim u_\tau. \tag{3.12}$$

Equations (3.5) and (3.9) are utilised in the above expressions. Owing to the assumed local homogeneity in the tangential direction, $\partial(\ )/\partial x_t \to 0$ and $\partial(\ )/\partial x_p = 0$ due to symmetry in the transverse direction for the conditional averages. Consequently, the tangential momentum balance is then stated as

$$U_n \frac{\partial U_t}{\partial x_n} = \nu \frac{\partial^2 U_t}{\partial x_n^2} - \frac{\partial \overline{u_t' u_n'}}{\partial x_n}. \tag{3.13}$$

Integration of (3.13) from the turbulent to the non-turbulent side results in the third superlayer jump condition of Reynolds (1972) after neglecting the viscous stress. We adhere to the differential form of (3.13) because within the superlayer the viscous effects are expected to be significant even if they are not in the turbulent and non-turbulent regions. If the viscous term in (3.13) is neglected then one gets a trivial solution. On the other hand if the gradient of shear stress is neglected then the transfer of momentum from the non-turbulent to the turbulent side is solely by viscous diffusion. The typical rates of entrainment observed in a TNTI cannot be explained by the viscous diffusive process while considering the Reynolds-averaged equations in the laboratory frame (since the advective flux of mean momentum is much larger than the diffusion especially at high *Re*). Hence, both terms on the right-hand side of (3.13) are deemed important to the superlayer dynamics.

Now consider a velocity scale v as the characteristic velocity of the turbulent motions within the superlayer such that $\overline{u_i' u_i'}/3 \sim v^2$ and ℓ as a length scale that is appropriate for the width of the superlayer. Considering the largest scale of motions within the interface will be of the order of the superlayer width, ℓ is the characteristic

length of the turbulent motions within the superlayer. Also the tangential velocity changes by $\mathcal{D}[U_t]$ across the superlayer. The approximation $\partial U_t/\partial x_n \approx -\mathcal{D}[U_t]/\ell$ is then appropriate. Using (3.11) we have an order of magnitude estimate for the convective transport and viscous diffusion terms in (3.13);

$$U_n \frac{\partial U_t}{\partial x_n} = O\left(u_\tau \frac{u_\tau}{\ell}\right), \tag{3.14}$$

$$\nu \frac{\partial^2 U_t}{\partial x_n^2} = O\left(\frac{\nu}{\ell}\frac{u_\tau}{\ell}\right). \tag{3.15}$$

Balance of the above two terms necessitates $\ell = O(\nu/u_\tau)$. The implication that the width of a thin region where viscous effects are important scales with a viscous length scale (ratio of ν and some characteristic velocity) should not be surprising as it is also the case for the scaling of the viscous sublayer width at the wall. On comparison of the stress-gradient term with the remaining we obtain

$$\overline{u_t' u_n'} = O(u_\tau^2). \tag{3.16}$$

The above order of magnitude estimate for $\overline{u_t' u_n'}$ stress is consistent with the typical argument $\overline{u_t' u_n'} \sim v^2$ in flows with shear. It is inferred that $v = O(u_\tau)$. It will be shown later regarding figure 7 that the order of magnitude for $\overline{u_t' u_n'}$ is indeed proper. The tangential momentum balance hence suffices in clarifying the scaling of $\overline{u_i' u_i'}$ and gives estimates of v and ℓ. We now examine the experimental data to verify these scaling behaviours.

3.3. *Experimental evidence*

In this section the experimental data are scrutinised for the validity of conclusions made in § 3.2. With the assumption of homogeneity in the tangential direction the conditionally averaged spanwise vorticity within the interface is expressed as

$$\langle \tilde{\Omega}_y \rangle \approx \frac{\mathrm{d}\langle \tilde{U} \rangle}{\mathrm{d}z}. \tag{3.17}$$

Figure 4(a) plots $\mathrm{d}\langle \tilde{U} \rangle/\mathrm{d}z$ normalised by U_∞/δ across the interface for the experimental data in lieu of spanwise vorticity. Note that the ordinate ξ is with reference to the interface position and is normalised by the boundary-layer thickness δ. All profiles show finite vorticity in the turbulent region and, as one moves outwards, the vorticity reaches a maximum and then drops to nearly zero in the non-turbulent region. The vorticity profiles show a bell-shaped behaviour in the region where it reaches its maximum. Such a narrow bell-shaped behaviour in the spanwise vorticity profile is the manifestation of a sharp jump in the velocity profile, similar to a delta function resulting for vorticity from a velocity jump modelled as a Heaviside function (Bisset *et al.* 2002; Westerweel *et al.* 2005). These characteristics along with figure 3(b) are evidence for the presence of a superlayer in the boundary layers analysed here. The vorticity profiles show two distinct Reynolds number trends. First, the peak of the vorticity magnitude that lies in the vicinity of $\xi = 0$ increases with increasing Reynolds number. Second, the width of the bell-shaped profile decreases with increasing Reynolds number (this is more evident on the non-turbulent side). It can be observed in figure 1(b) that the most significant change in the wall-normal
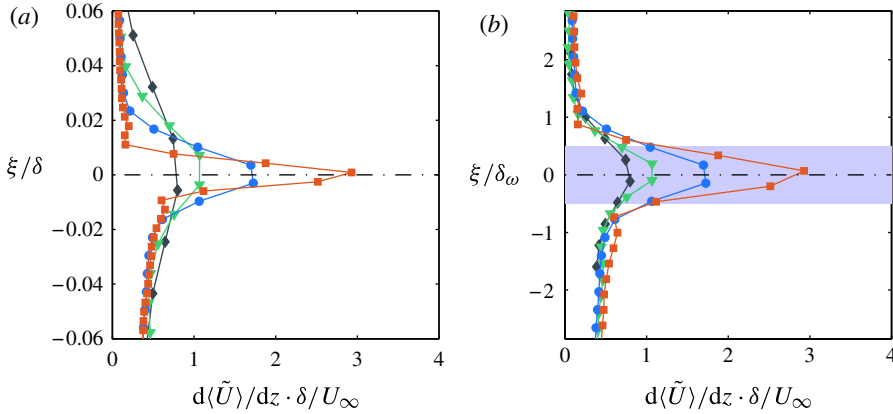
FIGURE 4. (Colour online) Spanwise vorticity calculated from conditionally averaged streamwise velocity, i.e. $\langle \tilde{\Omega}_y \rangle \approx d\langle \tilde{U} \rangle / dz$. See caption of figure 3 for symbol notations: (*a*) ξ normalised by δ; (*b*) ξ normalised by δ_ω. Shaded region is equivalent to the vorticity thickness δ_ω and is indicative of the superlayer.

gradient of $\langle \tilde{U} \rangle$ occurs over a region equivalent to the vorticity thickness. Therefore, the vorticity thickness δ_ω is determined for all four profiles using (1.1). (It is noted that due to the finite interrogation window size $d\langle \tilde{U} \rangle / dz$ is likely under-estimated and δ_ω is over-estimated. A finer resolution will then give a lower estimate of δ_ω. Hence, the value of δ_ω in this paper should be considered as the upper bounds for the vorticity thickness at the corresponding Reynolds numbers.) The ordinate ξ is then normalised by δ_ω and the vorticity profiles are re-plotted in figure 4(*b*). On normalisation of ξ by the vorticity thickness it is found that the profiles show a good agreement in the turbulent and the non-turbulent regions except for a narrow region in between where the vorticity peaks. In the region $-0.5 \lesssim \xi/\delta_\omega \lesssim 0.5$ (the shaded region), the vorticity profile for each Reynolds number peaks with the bell-shaped behaviour. The normalisation by vorticity thickness therefore takes away the Reynolds number trend of the changing width of the bell shape in $d\langle \tilde{U} \rangle / dz$ profiles. It is then concluded that the width equivalent to one δ_ω is a good measure of width of the superlayer.

In figure 4(*b*) the Reynolds number trend of increasing peak magnitude still remains. We note that the quantity $(d\langle \tilde{U} \rangle / dz)^{-1}$ indicates a time scale for the mean flow. The most rapid changes in the mean flow will occur when $d\langle \tilde{U} \rangle / dz$ is maximum. Hence, the peak magnitude in figure 4(*b*) and thereby $(d\langle \tilde{U} \rangle / dz|_{max})^{-1}$ represents a time scale over which rapid variation in mean flow occurs. If local self-preservation exists in the superlayer, then the turbulence therein will respond to the changes in the mean flow by keeping pace with it. In §3.2 we considered v and ℓ as the velocity and length scale, respectively, of the turbulence and it was concluded that $v \sim u_\tau$ and $\ell \sim \nu/u_\tau$. The turbulent time scale is then estimated as $\ell/v \sim \nu/u_\tau^2$. Considering the turbulent time scale and the mean flow time scale of the same order,

$$\left. \frac{d\langle \tilde{U} \rangle}{dz} \right|_{max} \sim \frac{u_\tau^2}{\nu} \Rightarrow \frac{\delta}{u_\tau} \cdot \left. \frac{d\langle \tilde{U} \rangle}{dz} \right|_{max} \sim \delta^+, \tag{3.18}$$
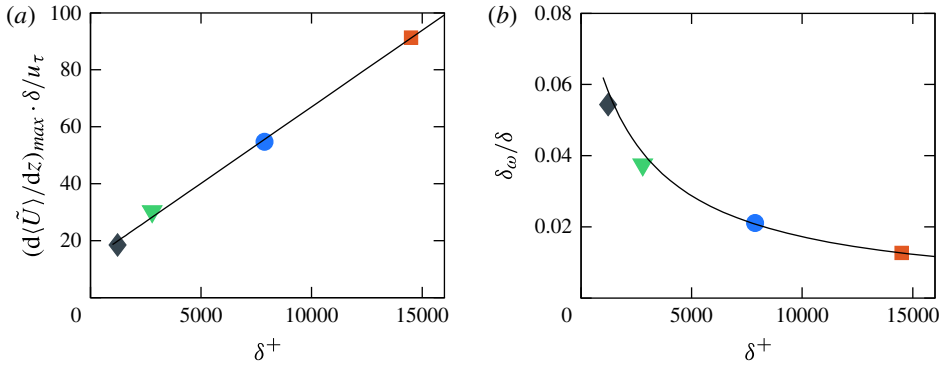
FIGURE 5. (Colour online) Reynolds number trends: (*a*) $(\mathrm{d}\langle \tilde{U}\rangle/\mathrm{d}z)_{max} \cdot \delta/U_\infty$; the solid line is (3.19); (*b*) δ_ω/δ; solid line is (3.20). See the caption of figure 3 for symbol notation.

which suggests that $\mathrm{d}\langle \tilde{U}\rangle/\mathrm{d}z|_{max}$ normalised by u_τ/δ scales linearly with Reynolds number δ^+. This behaviour is examined in figure 5(*a*) where $\mathrm{d}\langle \tilde{U}\rangle/\mathrm{d}z|_{max} \cdot \delta/u_\tau$ versus δ^+ is plotted. The maxima in the gradient of the conditional streamwise velocity profiles, i.e. $(\mathrm{d}\langle \tilde{U}\rangle/\mathrm{d}z)_{max}$ indeed shows a linear behaviour with δ^+ and supports the above reasoning. This linear behaviour is well indicated by the solid line on the figure and fitted with least squares:

$$\frac{\delta}{u_\tau} \cdot \left.\frac{\mathrm{d}\langle \tilde{U}\rangle}{\mathrm{d}z}\right|_{max} = a_1\,\delta^+ + a_2, \quad \text{with } a_1 = 5.4 \times 10^{-3}, \ a_2 = 13.23. \tag{3.19}$$

Also it is seen from the experimental data (see the inset in figure 3*b*) that the jump in the streamwise velocity $\mathcal{D}[\langle \tilde{U}\rangle]$ is approximately invariant with Reynolds number, i.e. $\mathcal{D}[\langle \tilde{U}\rangle] = b_1\,u_\tau$ ($b_1 \approx 1.15$). Utilising (3.9) and (3.19) in the definition of δ_ω we can write

$$\frac{\delta_\omega}{\delta} = \frac{b_1}{a_1\,\delta^+ + a_2}. \tag{3.20}$$

The vorticity thickness calculated from the experimental data is plotted versus δ^+ in figure 5(*b*) along with (3.20). (As noted earlier, the estimates of vorticity thickness here are considered as upper bounds due to the finite resolution in measurements. The linear trend in (3.18) is deduced from theoretical arguments and, hence, data from finer resolution measurements are also expected to adhere to the linear trend.) The vorticity thickness relative to the boundary-layer thickness decreases with increasing Reynolds number. The empirical (3.20) duplicates this behaviour very well in agreement with the experimental data. The trend for δ_ω/δ in figure 5(*b*) suggests that at very high Reynolds numbers the vorticity thickness and thereby the width of the superlayer is small compared with the boundary-layer depth. Equations (3.19) and (3.20) incorporate normalisation by the outer length scale δ, however, turbulent motions that are $O(\delta)$ are unlikely to have a viscous influence in the superlayer. Furthermore, the order of magnitude balance of the tangential momentum equation suggests that $\ell = O(\nu/u_\tau)$. Therefore, (3.19) and (3.20) are posed using the inner
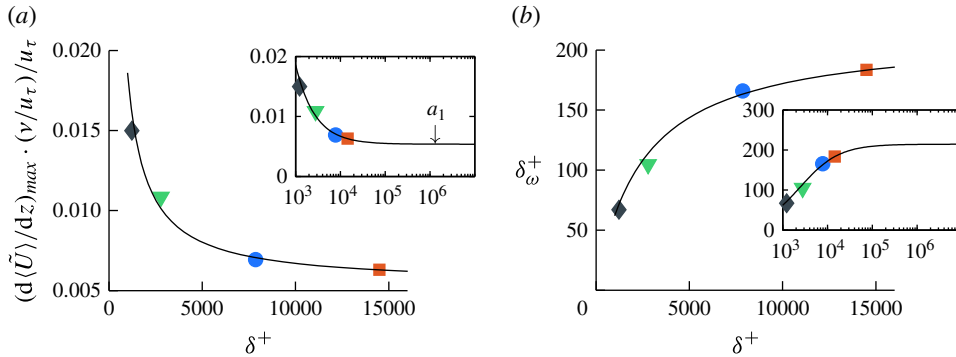
FIGURE 6. (Colour online) Reynolds number trends: (*a*) $(\mathrm{d}\langle\tilde{U}\rangle/\mathrm{d}z)_{max} \cdot (v/u_\tau)/U_\infty$; the solid line is (3.21); (*b*) δ_ω^+; solid line is (3.22). See the caption of figure 3 for symbol notation.

normalisation by v/u_τ instead of δ as below:

$$\frac{v/u_\tau}{u_\tau} \cdot \frac{\mathrm{d}\langle\tilde{U}\rangle}{\mathrm{d}z}\bigg|_{max} = a_1 + \frac{a_2}{\delta^+} \tag{3.21}$$

$$\frac{\delta_\omega u_\tau}{v} = \delta_\omega^+ = \frac{b_1}{a_1 + a_2/\delta^+}. \tag{3.22}$$

Figure 6(*a,b*) show variation of $(\mathrm{d}\langle\tilde{U}\rangle/\mathrm{d}z)_{max}$ and δ_ω, respectively, with Reynolds number, normalised with v/u_τ as the length scale. The experimental data is plotted and compared with expressions (3.21) and (3.22). A good agreement is seen between the empirical forms and the experimental data throughout the Reynolds number range. Further it is noted that the form of (3.21) and (3.22) is such that in the limit of high Reynolds number, i.e. $\delta^+ \to \infty$, they asymptote to a constant. This asymptotic limit is a_1 for the maxima in the gradient of the conditional streamwise velocity profile that is normalised by $u_\tau/(v/u_\tau)$. The extrapolation of (3.21) shows this limit in the inset to figure 6(*a*). On the other hand the asymptotic limit for δ_ω^+ is $b_1/a_1 \approx 215$, which is again shown via extrapolation of (3.22) in figure 6(*b*).

These high-Reynolds-number limits are encouraging, in particular for δ_ω as it is in agreement with the conclusion made from the order of magnitude of the tangential momentum balance in §3.2, i.e. the asymptotic invariance of δ_ω^+ in the limit $\delta^+ \to \infty$ implies that $\delta_\omega \sim v/u_\tau$. Earlier it was also deduced in §3.2 that $\ell \sim v/u_\tau$, where ℓ was considered as the characteristic length scale of the turbulent motions that span the width of the superlayer. The experimental data seen so far indicate that δ_ω is an effective length scale to characterise this width (scaling ξ by δ_ω in figure 4(*b*) concentrates the bell-shaped discontinuity in spanwise vorticity within a region equivalent to one δ_ω). Thereby $\ell \simeq \delta_\omega$ is appropriate.

In the preceding discussion regarding the turbulent time scale we considered $v \sim u_\tau$ based of the order of magnitude analysis of §3.2. Support for this scaling is also found in the following arguments. Corrsin & Kistler (1955) explains that the non-turbulent flow acquires vorticity through diffusion, which in turn is amplified by vortex stretching by the vorticity and mean shear that exists on the turbulent side. The streamwise velocity profiles resembling a shear layer in figure 3(*b*) assist in vortex
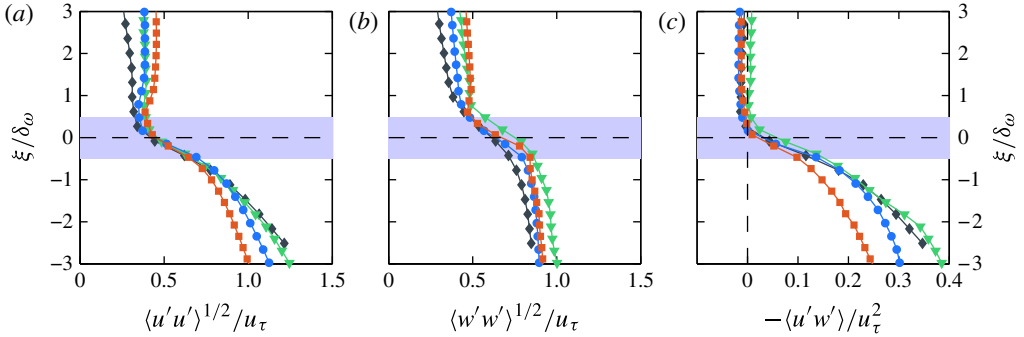
FIGURE 7. (Colour online) Conditionally averaged statistics with respect to the interface location z_i: (a) r.m.s. of streamwise fluctuations $\langle u'u' \rangle^{1/2}$; (b) r.m.s. of wall-normal fluctuations $\langle w'w' \rangle^{1/2}$; (c) Reynolds shear stress $-\langle u'w' \rangle$. The shaded region in each panel is equivalent to the vorticity thickness δ_ω and is indicative of the superlayer. See the caption to figure 3 for symbol notation.

stretching. One can also model the bell-shaped behaviour of spanwise vorticity in figure 4(b) using a Gaussian function, analogous to the vorticity in an Oseen vortex. In addition, da Silva & Taveira (2010) have observed that coherent vortices are present at the TNTI that are comparable with the interface thickness in size. Based on these observations it is likely that a certain vortex-like feature or vortex sheet resides within the superlayer. Considering the interface is populated with vortices or vortex-like motions, the angular momentum of such motions is conserved such that

$$v \cdot \ell \sim \text{constant}. \tag{3.23}$$

On substituting $\ell \simeq \delta_\omega$, which in turn scales with ν/u_τ, we obtain

$$v \sim u_\tau. \tag{3.24}$$

Equation (3.24) arrives at the same conclusion that $v \sim u_\tau$ by the argument of conservation of angular momentum.

At this point inspection of experimental results for the scaling of the turbulent velocity fluctuations within the superlayer is duly required. Fluctuating components of streamwise and wall-normal velocities are calculated with respect to the conditional mean profiles in figure 3. Using these fluctuating components, figure 7(a,b) plots the conditional profiles of $\langle u'u' \rangle^{1/2}/u_\tau$ and $\langle w'w' \rangle^{1/2}/u_\tau$, respectively. We adhere to the normalisation of the ordinate ξ by the vorticity thickness, δ_ω. The profiles of both standard deviations undergo a sudden rise in the region that is marked as the superlayer as one moves from the non-turbulent region to the turbulent region. The root-mean-square (r.m.s.) profiles when scaled with u_τ exhibit very good collapse within the superlayer for a range of $\delta^+ = 1200$–$14\,500$. This agreement implies that the fluctuations within the superlayer scale with u_τ and the conclusion made in § 3.2 that $v \sim u_\tau$ is thus validated again. Using the fluctuations with respect to the conditional mean, figure 7(c) plots the conditional Reynolds shear stress, $-\langle u'w' \rangle$ normalised by u_τ^2. All profiles indicate that the Reynolds shear stress is virtually zero in the non-turbulent region and it sharply rises within the superlayer to reach finite magnitude in the turbulent region. Within the superlayer the profiles show good

agreement and a lack of Reynolds number trend. The profile for $\delta^+ = 14\,500$ deviates from the rest in the turbulent region ($\xi/\delta_\omega < -0.5$), however scaling in this region is not the concern of this study. This agreement supports the scaling of the Reynolds shear stress by u_τ^2 and substantiates our interpretation of the superlayer dynamics from the governing equations in § 3.2.

4. Discussion

In this section we undertake a discussion on these scales to interpret the significance of the TNTI for turbulent boundary layers as a whole.

4.1. *The velocity scale* u_τ

We have observed that a sharp jump in the tangential velocity occurs at the superlayer which also scales with u_τ. To explain the emergence of this scaling we turn to the third superlayer jump condition obtained by Reynolds (1972), which for the control volume illustrated in figure 2(c) is written as

$$U_n \, \mathcal{D}[U_t] = (\overline{u'_t u'_n})^t. \tag{4.1}$$

Here $(\overline{u'_t u'_n})^t$ is the Reynolds shear stress on the turbulent side of the superlayer. Since $(\overline{u'_t u'_n})^t$ is finite and so is U_n, the tangential mean velocity U_t exhibits a discontinuity across the superlayer. It is noted that Reynolds (1972) did not conclude that a discontinuity occurs at the superlayer. However, (4.1) is still valid across the superlayer as it is obtained after integration of the tangential momentum balance and applying the boundary conditions, doing so without an assumption of discontinuity in U_t. We know that U_n scales with u_τ in the boundary layer and if $(\overline{u'_t u'_n})^t \sim u_\tau^2$, then $\mathcal{D}[U_t] \sim u_\tau$. The scaling of $(\overline{u'_t u'_n})^t$ with u_τ^2 is evident in figure 7(c) and follows from the fact that the skin-friction velocity serves as the velocity scale for mean velocity deficit and the turbulent stresses in the outer region (Marusic, Uddin & Perry 1997; Smits, McKeon & Marusic 2011). The validity of u_τ as the velocity scale for fluctuations in the outer-scaling (z/δ) is also obvious from figure 8(a), which plots the r.m.s. of the streamwise velocity fluctuations (u, in the laboratory frame) in the intermittent region of the boundary layer. (The normal stress $\overline{uu}$ is examined here as it is more pertinent to the discussion of Kolmogorov and Taylor scales and accurately available from hot-wire measurements over a wide range of Reynolds numbers.) The r.m.s. is also calculated from only the turbulent segments of the signal utilising the fluctuations that are relative to the mean in the turbulent regions. The turbulent/non-turbulent zones in a hot-wire signal are identified using $(1 - \tilde{U}/U_\infty)^2$ as the detector function (Chauhan *et al.* 2014). Over the range of Reynolds number plotted in figure 8(a), the collapse of profiles indicates that throughout the intermittent region u_τ is an appropriate velocity scale for the fluctuations of the whole signal or just the turbulent parts, i.e. one can write

$$\overline{uu}^{1/2}(z/\delta) = u_\tau \, g_o(z/\delta). \tag{4.2}$$

Here $g_o(z/\delta)$ is the outer similarity profile for the streamwise intensity that is independent of Reynolds number and valid in and above the overlap region. In fact, the r.m.s. for only the turbulent zones in figure 8(a) is approximately equal to u_τ in the region $z/\delta > 2/3$. Hence, even in the regions where mostly non-turbulent flow exists, the turbulence within the short-lived turbulent zones is still of the order of u_τ.
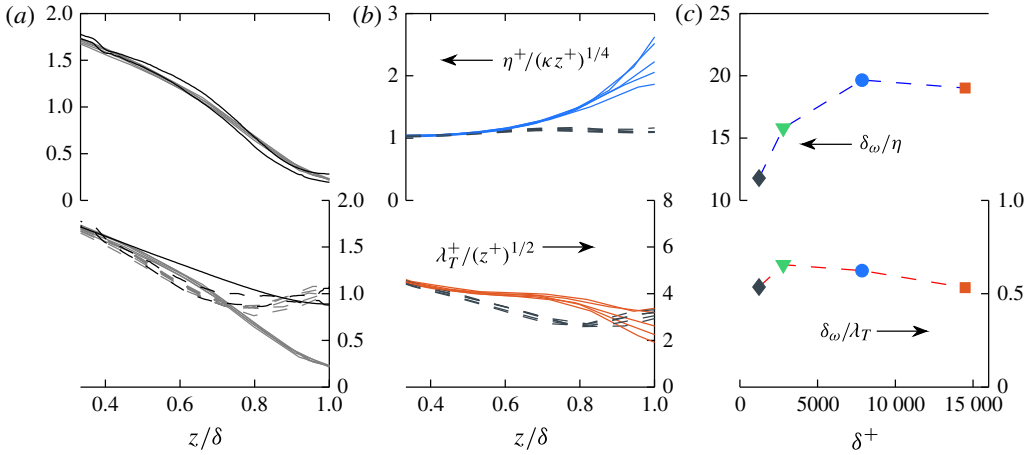
FIGURE 8. (Colour online) Scales of turbulent motions in the intermittent region ($1/3 \leqslant z/\delta \leqslant 1$). (*a*) Root mean square of the streamwise velocity fluctuations. Top: solid (grey) lines, hot-wire data of Hutchins *et al.* (2009) ($\delta^+ \approx 2800\text{--}19\,030$); solid (black) lines, present PIV data. Bottom: $\overline{uu}^{1/2}/u_\tau$ calculated in the turbulent zones only; dashed (grey) lines, hot-wire data of Hutchins *et al.* (2009); dashed (black) lines, present PIV data. Solid (grey) lines, $\overline{uu}^{1/2}/u_\tau$ calculated from the full signal (duplicated from the plot on top). Solid (black) line, $\overline{uu}^{1/2}/u_\tau$ for the channel flow data of Hoyas & Jiménez (2006) at $Re_\tau = 2003$. (*b*) Solid (blue online) lines, $\eta^+/(\kappa z^+)^{1/4}$ on top; solid (red online) lines, $\lambda_T^+/(z^+)^{1/2}$ on bottom. Corresponding dashed lines indicate that the quantities are calculated from the turbulent zones only. (*c*) Vorticity thickness scaled by Kolmogorov and Taylor scales (from the full signal) at $z/\delta = 2/3$ at corresponding Reynolds numbers of the four data sets. See the caption to figure 3 for symbol notation.

Note that the r.m.s. of the streamwise fluctuations in the turbulent zones are of the same order of magnitude as the r.m.s. in a turbulent channel flow (solid black line).

Equation (4.2) is not new in boundary-layer research and follows from Townsend's Reynolds number similarity hypothesis which is stated as (Townsend 1956, p. 89):

> 'In a fully turbulent flow, there exists a region including almost all of the flow, over which the direct action of viscosity on the mean flow is negligible, i.e. the Reynolds stresses are large compared with the mean viscous stresses. Within this region, the mean motion and the motion of the energy-containing components of the turbulence are determined by the boundary conditions of the flow alone, and are independent of the fluid viscosity, except so far as a change in the fluid viscosity may change the boundary conditions.'

To elaborate on the implications of the above hypothesis for TNTI we consider a fully developed turbulent boundary layer (a flow that has no memory of its history) at a fixed streamwise location under constant free-stream velocity. This flow is bounded by two boundaries, one is the wall and the other is the non-turbulent flow residing above it. The boundary condition at the wall is set within the viscous sublayer such that $u_\tau^2 = \nu(\mathrm{d}U/\mathrm{d}z)|_{z=0}$. The scaling of fluctuations in figure 8(*a*) by u_τ is therefore consistent with the notion that mean motion (not shown here) and the turbulence are determined by the gradient at the wall. Now if by some means the fluid viscosity is

changed, an immediate response of the boundary layer occurs at the wall resulting in a change in u_τ ($\mathrm{d}U/\mathrm{d}z|_{z=0}$ also changes), which is equivalent to a change in the boundary condition. The bulk flow (the log region and beyond) and the turbulent motions within will then adjust accordingly such that fluctuations will scale with u_τ, i.e. $(\overline{u'_t u'_n})^t \sim u_\tau^2$ and thereby $\mathcal{D}[U_t] \sim u_\tau$ from (4.1). According to Reynolds number similarity, the change in *Re* brought on by changing the viscosity is equivalent to varying the *Re* by changing U_∞ or *x*. Since the scaling by u_τ is specific to the case of a turbulent boundary layer (as opposed to turbulent jets/wakes where the wall is absent), Townsend's hypothesis explains the influence of the wall on the finite velocity jump.

Furthermore, utilising the tangential momentum balance we deduce that the velocity scale (v) for turbulent fluctuations within the interface is also u_τ. Our interpretation of (3.16) finds experimental support in figure 7 for the r.m.s. of fluctuations and the corresponding Reynolds shear stress in a frame of reference relative to the interface. The turbulent velocity scale v is determined by the jump in the tangential velocity $\mathcal{D}[U_t]$ across the interface which scales with u_τ. Such a scaling behaviour is analogous to shear layers and wakes, where the turbulent velocity fluctuations scale with the maximum mean velocity defect. This similarity is further considered in §4.3.

A satisfactory dynamical basis for the scaling of the fluctuations by u_τ is also obtained through the conservation of angular momentum (3.23) by considering v/u_τ as the characteristic length scale of turbulent motions in the superlayer. Since the turbulent motions that span the width of the layer are typically filamentary vortices that undergo stretching in the presence of the local shear (da Silva & dos Reis 2011) the conservation of angular momentum is applicable to such structures.

Before concluding this subsection on u_τ scaling it is also interesting to note that an analysis that was suggested to the authors by an anonymous referee allows an appraisal of the scaling of the fluctuating spanwise velocity of the TNTI. The details of this analysis are given in appendix A, where given the definition that the instantaneous velocity of the TNTI utilising Reynolds decomposition is $\boldsymbol{v}_I = (U_I + u'_I, W_I + w'_I, V_I + v'_I)$ in the (x, z, y) directions, respectively, the spanwise fluctuations $v'_I = O(u'_I) = O(u_\tau)$. The scaling $v'_I = O(u_\tau)$ is analogous to the scaling of spanwise fluctuations of the fluid velocity $\overline{vv}^{1/2} \sim u_\tau$ (e.g. Jiménez & Hoyas 2008; Bernardini, Pirozzoli & Orlandi 2014).

4.2. *The length scale v/u_τ*

It can be argued that u_τ is the velocity scale that is responsible for setting v/u_τ as the length scale. From figure 8(*a*) we know that turbulent motions in the outer part scale with u_τ. As diffusion of vorticity has to occur from the turbulent region towards the non-turbulent regions, the spatial extent of these diffusing motions will be viscosity dependent. An eddy with a characteristic velocity u_τ will then diffuse over a length v/u_τ in the characteristic time of v/u_τ^2. Previous studies, for example those of Falco (1977), Head & Bandyopadhyay (1981) and Murlis, Tsai & Bradshaw (1982), have also observed that the vortical features in the outer region of the boundary-layer scale with the viscous length scale v/u_τ (it is noted that these studies did not explicitly identify vortical features in the vicinity of the interface and their findings apply to the complete outer region).

The theoretical estimate of the length scale of turbulent motions in our study is an indirect one. We deduce that the turbulent motions within the superlayer scale with the viscous length scale by considering the viscous diffusion to be of significance in the

tangential momentum balance. The viscous influence applies to the jump in tangential velocity across the interface, where the diffusive nature of viscosity tends to smooth out any discontinuities in the velocity distribution. We recall Townsend's similarity hypothesis stated in the previous subsection, now applying it to the TNTI. The viscous superlayer will adjust to a change in viscosity by varying the extent and magnitude of the velocity gradient of the jump, similar to the change in the gradient $(\mathrm{d}U/\mathrm{d}z)|_{z=0}$ in the viscous sublayer. Therefore, a viscous length scale is appropriate to characterise the scaling of the TNTI dynamics with varying Reynolds number. The viscous scale ν/u_τ deduced here for the thickness of the interface and motions within is consistent with the similarity hypothesis.

In recent literature, the width of the region where the mean vorticity peak occurs is found to be of the order of Taylor microscale (e.g. Bisset *et al.* 2002; da Silva & Taveira 2010), while here we find it to scale with ν/u_τ. Figure 8(*b*) plots the Kolmogorov scale η (top) and the Taylor microscale λ_T (bottom) normalised by $(\nu/u_\tau)(\kappa z^+)^{1/4}$ and $(\nu/u_\tau)(z^+)^{1/2}$, respectively, in the intermittent region of the boundary layer. The proportionality $\eta^+ \sim (\kappa z^+)^{1/4}$ follows from the assumption that the production of turbulent KE equals the dissipation and $-\overline{uw}/u_\tau^2 \approx 1$ in the logarithmic region (e.g. Pope 2000), while an additional assumption $\overline{uu}/u_\tau^2 \approx$ constant results in $\lambda_T^+ \sim (z^+)^{1/2}$ (Marusic & Adrian 2012). Hot-wire measurements of Hutchins *et al.* (2009) over a range of $\delta^+ = 2800$–$19\,030$ are utilised in figure 8(*b*). The length scales are calculated using Taylor's hypothesis to evaluate $\partial u/\partial x$ from $\partial u/\partial t$ and isotropy assumptions are employed to estimate the dissipation. The following relations are used to estimate η and λ_T from hot-wire data:

$$\eta = \left(\frac{\nu^3}{\epsilon}\right)^{1/4}, \quad \text{where } \epsilon = 15\nu\overline{\left(\frac{\partial u}{\partial x}\right)^2}, \quad \text{and} \quad \lambda_T^2 = \overline{uu}\left[\overline{\left(\frac{\partial u}{\partial x}\right)^2}\right]^{-1}. \quad (4.3a,b)$$

In the intermittent region η and λ_T are also calculated using only the turbulent segments of the signal (shown by the dashed lines) in order to examine the influence of non-turbulent zones in the estimation of these scales. It is seen that profiles for $\eta^+/(\kappa z^+)^{1/4}$ show a very good collapse for $z/\delta < 0.8$ over the *Re* range. The profiles evaluated only in the turbulent zones show a remarkable collapse throughout the intermittent region and the ratio $\eta^+/(\kappa z^+)^{1/4}$ continues to remain approximately equal to one. Similarly the profiles for $\lambda_T^+/(z^+)^{1/2}$ calculated from the full velocity signal shows a good collapse up to $z/\delta \approx 0.7$, while the profiles calculated from only the turbulent segments show *Re*-independence throughout the intermittent region. It is then obvious that at a particular reference height (e.g. $z/\delta = 2/3$, the mean interface location) in the intermittent region, $\eta^+(z/\delta) \sim (\delta^+)^{1/4}$ and $\lambda_T^+(z/\delta) \sim (\delta^+)^{1/2}$, implying that the change of η^+ and λ_T^+ with Reynolds number is noticeably small. Over the range of Reynolds number considered in this study (a decade of δ^+), at the mean interface location, the ratio of Taylor microscale to the viscous scale, i.e. $\lambda_T/(\nu/u_\tau)$ changes by a factor of approximately 3 while the ratio of Kolmogorov scale to the viscous scale, i.e. $\eta/(\nu/u_\tau)$, changes by a factor of approximately 1.8. Utilising the values of η and λ_T at the mean interface location for the four Reynolds numbers considered here, figure 8(*c*) plots the ratio of the vorticity thickness δ_ω at the TNTI to these scales. It is seen that δ_ω/η increases at low Reynolds numbers and the trend reaches an approximate constant value at high Reynolds number. This trend is similar to the trend observed for $\delta_\omega/(\nu/u_\tau)$ owing to the gradual variation in $\eta/(\nu/u_\tau)$. On the other hand, the ratio δ_ω/λ_T (bottom plot of figure 8*c*) does not vary

significantly. Previous studies by Bisset *et al.* (2002) and da Silva & Taveira (2010) in free-shear flows have concluded that $\delta_\omega = O(\lambda_T)$. Our findings are consistent with these observations. As an interesting aside, if we consider $\lambda_T \approx \delta_\omega$, then the Reynolds number based on the Taylor microscale $Re_\lambda \approx \delta_\omega^+$ (with u_τ as the characteristic velocity fluctuation) inside the superlayer, and range of δ_ω^+ in figure 6(*b*) corresponds to that observed at the mixing transition (e.g. Dimotakis 2005). This suggests that when the non-turbulent fluid becomes turbulent after crossing the interface, in the immediate vicinity of the interface the flow rapidly becomes fully turbulent. This is in accordance with the findings of da Silva & Pereira (2008) where they observe fully turbulent features close to the interface.

Now, two considerations should then be taken into account for figure 8(*c*). First, if we assume that the Kolmogorov length is the true length scale to characterise the superlayer width; then this assumption is consistent with the scaling originally proposed by Corrsin & Kistler (1955); also see Sreenivasan *et al.* (1989*a*) and Holzner *et al.* (2008). Since $\eta^+(z/\delta) \sim (\delta^+)^{1/4}$, the scaling by η or ν/u_τ is indistinguishable in the measurements analysed here. At low δ^+ the flow is not fully developed and thus the variation of δ_ω^+ (or δ_ω/η) is possibly a manifestation of the low-*Re* behaviour of $C_f = 2u_\tau^2/U_\infty^2$ (Monkewitz, Chauhan & Nagib 2007) and/or the lack of sufficient scale separation between η and δ. Second, if however we assume that the Taylor microscale is the true length scale for superlayer width, seemingly apparent from figure 8(*c*, bottom); then in this case the characteristic velocity scale is $\overline{uu}^{1/2}$ which is proportional to u_τ. The width of the layer is then determined by velocity scale u_τ (via $\overline{uu}^{1/2}$) and a local viscous influence at the TNTI. Noting that $\lambda/\eta \sim (\delta^+)^{1/4}$ at a fixed z/δ, the validation of these two equally justifiable assumptions require measurements over an even wider range of Reynolds number than presented here. Hence, the present experimental data are not definitely conclusive regarding the role played by η and λ in the scaling of the TNTI as compared with scaling by ν/u_τ. It is noted, that using ν/u_τ and u_τ as the relevant length and velocity scales over Taylor and Kolmogorov scales in a boundary layer has an advantage as u_τ and ν are known *a priori*.

Earlier a peculiar behaviour was observed in figure 8(*b*) for the ratio $\eta^+/(\kappa z^+)^{1/4}$ calculated in turbulent zones only in the form of the ratio being approximately equal to one through the intermittent region for all Reynolds numbers. This similarity of Kolmogorov scales in the intermittent turbulent region to the Kolmogorov scales near the wall is possibly a signature of their association. It is plausible that the structure of turbulence in the turbulent zones of the intermittent region is either determined by the near wall turbulence or analogous to it. Such a scenario is possible in the description of Adrian (2007) wherein hairpin packets that are typically found in the lower half of the boundary layer (especially the logarithmic layer) possibly extend to the edge of the boundary layer to result in turbulent bulges. Furthermore, Morrill-Winter & Klewicki (2013) recently proposed that beyond the logarithmic region small-scale high-vorticity motions are spatially dispersed via the advective transport associated with $\overline{w\omega_y}$ (Taylor 1938). The dispersive nature of eddy structures in the logarithmic region is evident in the results of Herpin *et al.* (2013) where it is shown that the radius of spanwise vortices remain almost constant in the log layer when scaled with the local Kolmogorov scale. In either case, the growing packets or the advective high-vorticity motions obtain their characteristic velocity from the near-wall turbulence where they originate, and this characteristic velocity persists when these motions reach the outer region. These mechanisms are consistent with Townsend's hypothesis in explaining u_τ as the velocity scale of turbulence in the outer part of the boundary layer.
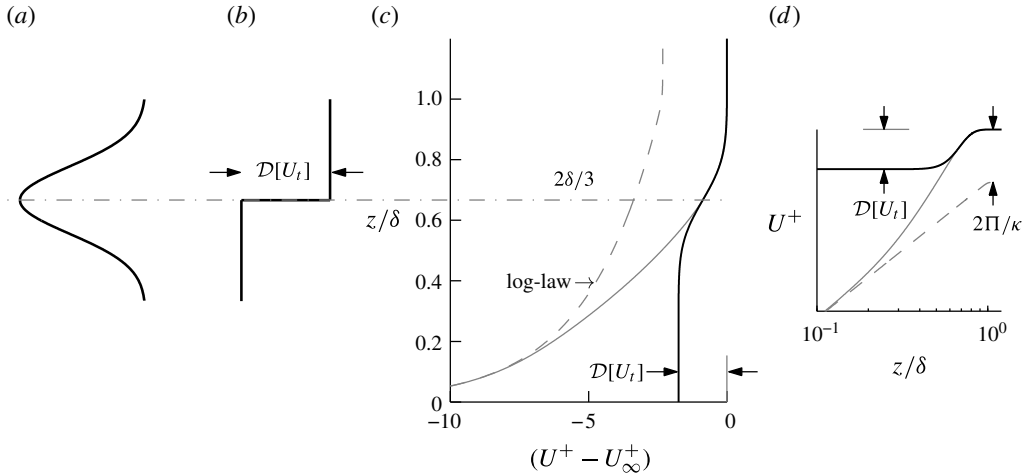
FIGURE 9. (*a*) Gaussian p.d.f. of interface location z_i. The mean is at $2\delta/3$ and standard deviation is $\delta/9$. (*b*) Superlayer jump in streamwise velocity modelled as a step function. (*c*) Solid (grey) line, mean velocity deficit $U^+ - U_\infty^+$; solid (black) line, convolution of a step function and a Gaussian distribution; dashed (grey) line, deficit log law. (*d*) Mean velocity profile U^+ corresponding to the deficit in (*c*).

4.3. *On the superlayer and the boundary-layer wake region*

We have deduced that the turbulent velocity scale is u_τ and also concluded that the mean velocity deficit within the superlayer scales with u_τ. It is inferred that the turbulent KE within the superlayer is prescribed by the velocity deficit, the deficit being of the order of u_τ (3.11). This characteristic is similar to the scaling of velocity fluctuations in a two-dimensional turbulent far-wake. In the far-wake region it is known that $v/U_s = O(1)$, where U_s is the velocity deficit at the centreline of the wake (Tennekes & Lumley 1972). Although the average structure of the mean velocity profile across the superlayer resembles a mixing-layer profile, in the aspect of its turbulent velocity scale v being of the same order has the deficit $\mathcal{D}[\langle \tilde{U} \rangle]$, the superlayer can be considered wake-like locally, albeit 'half-wake'.

It then follows to examine whether this localised wake behaviour manifests itself in some way onto the mean boundary-layer structure. The indirect influence of viscosity via the superlayer on the mean in the intermittent region of the boundary layer has been previously considered by Coles & Hirst (1968) and Huffman & Bradshaw (1972). In particular, Kovasznay (1967) and Huffman & Bradshaw (1972) noted that in pipe and duct flows a TNTI is not present. The agreement of the r.m.s. profile from turbulent channel flow data of Hoyas & Jiménez (2006) with the r.m.s. of fluctuations within the turbulent zones only for a boundary layer in figure 8(*a*) points to this difference. Huffman & Bradshaw (1972) also proposed that in a developing boundary layer at low Reynolds number, the presence of the viscous superlayer in the intermittent region is responsible for the low-*Re* development of wake parameter Π observed in experimental data (Coles & Hirst 1968; Chauhan *et al.* 2009). Keeping the scaling relations obtained so far at hand, we shall identify the influence of the superlayer, in particular the sharp velocity jump on the mean velocity profile.

A sharp change in velocity occurs at the interface over a wall-normal distance of the order of δ_ω and at high Reynolds numbers $\delta_\omega/\delta \to 0$. In the high-*Re* limit, this sharp change can be modelled as a step change in velocity as shown in figure 9(*b*)

(e.g. Westerweel *et al.* 2005; Chauhan *et al.* 2014). This step change in velocity flutters across the boundary layer along with the instantaneous interface location z_i. The probability distribution of the instantaneous interface location z_i is well represented by a Gaussian distribution (Townsend 1976), the span of which scales with δ (e.g. Corrsin & Kistler 1955; Chauhan *et al.* 2014). The probability distribution function (p.d.f.) is illustrated in figure 9(*a*). Thereby the resultant velocity distribution can be estimated by taking a correlation between the step change in the streamwise velocity and the Gaussian probability distribution of its location, i.e. the conditional (step) velocity profile scans the Gaussian p.d.f. The ensuing velocity profile in the defect form is plotted in figure 9(*c*) in comparison with the mean velocity defect in a zero-pressure-gradient turbulent boundary layer. The mean deficit profile is plotted using the composite velocity profile of Chauhan *et al.* (2009) and is *Re*-independent in the outer part. Nee & Kovasznay (1969) have used similar 'smearing' of the total turbulent viscosity by the Gaussian distribution in the boundary layer to achieve a good agreement for the mean velocity profile in the outer part.

It is found that the deficit profile emerging from the existence of a superlayer jump is in excellent agreement with the mean deficit profile of the boundary layer for the region $z/\delta > 0.6$ that is 40 % of the boundary layer in the outer part. In figure 9 we have chosen $\mathcal{D}[U_t]/u_\tau = -1.75$ which is equal to twice the value of $U^+ - U_\infty^+$ at $z/\delta = 2/3$ (the choice of the reference location is arbitrary and here taken as the mean interface location). Hence, a direct dynamical influence of Corrsin's superlayer on Coles' wake profile is demonstrated here in a quantitative manner. In the region below ($z/\delta < 0.6$), the intermittency is greater than 0.5 and therefore the mean profile would have a dominating influence of the gradient dU/dz in the turbulent part which is unaccounted for in figure 9. Understandably the profile obtained from the step function does not agree well with the mean velocity deficit in this region. If a gradient is prescribed for the turbulent part in figure 9(*b*), then the resultant correlation profile might agree further deep into the boundary layer. However, we refrain from introducing empiricism by specifying the gradient magnitude, because the TNTI is not the only shear layer (step function) but there are also other instantaneous shear layers inside the turbulent boundary layer (Meinhart & Adrian 1995) which would have to be taken into account for a fuller explanation of the wake.

4.4. *Implications for other wall-bounded flows*

As can be seen in figure 9(*d*), the jump $\mathcal{D}[U_t]$ is slightly smaller than the wake strength $2\Pi/\kappa$, the difference being 0.57. This difference is equivalent to a wake parameter $\Pi = 0.11$ (with $\kappa = 0.384$), which is within the range of Π values observed in pipes and channels ($\Pi \approx 0.05$ for turbulent channel flows and $\Pi \approx 0.2$ for pipe flows; see Nagib & Chauhan (2008)). Since the wake profile in boundary layers is observed above $z/\delta \approx 0.15$, while the intermittency resides above $z/\delta \approx 0.3$, it is evident that the wake profile is not solely due to the wake-like TNTI and that it is also influenced by the turbulence below. Similarly a wake profile is present in turbulent pipes and channels even though a strict TNTI is not present in these flows. Hence, in turbulent pipes, channels and boundary layers, a certain phenomenon that is different from the TNTI but common to these flows causes the mean velocity profile to deviate from the log law in the outer region. While a deviation from the logarithmic profile in the outer part is observed in all canonical wall-bounded flows, the wake parameter in boundary layers is typically larger than pipes and channels. It is then safe to theorise that the additional contribution to the wake parameter in boundary layers is a result

of the presence of a superlayer across which a jump in tangential velocity (that is predominantly streamwise) occurs.

It is also important to consider the mean entrainment mechanism in non-canonical flows, even if qualitatively. In the case of a zero-pressure-gradient boundary layer over a rough surface, the local boundary layer thickness is higher compared to δ for a flow over a smooth wall under the same free-stream velocity at a particular streamwise location. This would imply that the mean entrainment rate has to increase to account for the increased mass-flux in a rough-wall boundary layer. This adjustment of the flow to surface roughness is explained by Townsend's outer flow similarity hypothesis for rough wall boundary layers. In essence the hypothesis states that for a turbulent flow over a uniformly distributed roughness, if the roughness height (k) is small compared to the boundary layer width (δ), then turbulence in the outer region is not affected by the nature of roughness and, as with a smooth wall, it will be determined by the average wall stresses, the layer depth and the fluid viscosity (p. 139 Townsend 1976). This hypothesis has been verified experimentally for various rough-wall geometries in many experimental studies, most recently by Schultz & Flack (2007) and Wu & Christensen (2007), to show that the turbulent fluctuations in the outer region scale with u_τ. (Also see the list of previous studies in Wu & Christensen (2007) that support or dispute the hypothesis.) Along with the increase in δ, a concurrent increase in u_τ occurs and, as per the discussion above, the turbulence in the outer part adjusts to the changed wall-boundary condition. Consequently the mean entrainment rate across the TNTI becomes consistent with the local turbulence level that scales with u_τ.

5. Summary

In order to advert a particular scaling data at different Reynolds numbers are examine for the TNTI in zero-pressure-gradient turbulent boundary layers. It is shown that the TNTI dynamics in boundary layers are influenced by the wall. The consequences of the wall boundary condition to the superlayer are explained via Townsend's similarity hypothesis and the mechanisms leading to observed scaling of TNTI with Reynolds number are summarised in figure 10(a). The mean entrainment corresponds to the growth of the boundary layer and results in u_τ as the velocity scale for the net entrainment velocity. Outer similarity of turbulent stresses imposes the Reynolds shear stress to scale with u_τ^2, which in turn results in the mean tangential velocity jump to scale with u_τ. The local turbulence is dictated by the velocity jump and the velocity fluctuations then scale with u_τ accordingly. The mean superlayer width is governed by the influence of viscosity on the tangential velocity jump. The influence of viscosity coupled with the velocity scale u_τ gives rise to the viscous length scale ν/u_τ as the characteristic length. The viscous length scale ν/u_τ is a utilitarian preference for the superlayer width and the motions within. Since the Kolmogorov scale and Taylor's microscale vary gradually relative to the viscous scale, the appropriateness of scaling by η or λ_T can only be clarified using a very wide range of Reynolds number. These conclusions are supported via conditional statistics from experiments.

The invariance of the superlayer width in viscous units, i.e. $\delta_\omega^+ \to$ constant at high Reynolds numbers, is analogous to the invariant depth of the viscous sublayer next to the wall in viscous scaling. Figure 10(b) illustrates the viscous *super*layer and the viscous *sub*layer for comparison. Three schematics are shown to depict a developing boundary layer (U_∞ is held constant) at low, moderate and high Reynolds number.
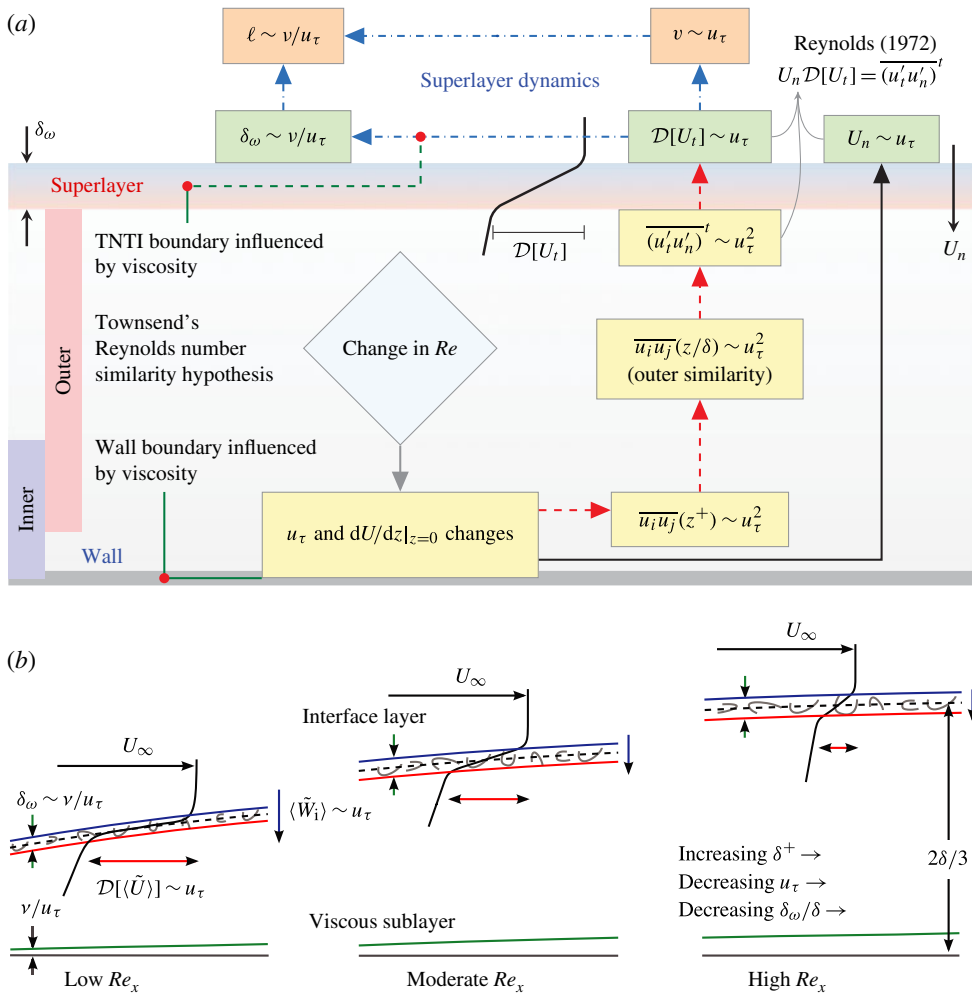
FIGURE 10. (Colour online) (*a*) Mechanisms leading to observed scaling of TNTI with Reynolds number in a boundary layer. Boxes show different scalings that exist. A change in Reynolds number changes u_τ at the wall. Near-wall motions and thereafter turbulence in the outer part scales accordingly with u_τ (dashed arrows, red online). The mean entrainment velocity changes with u_τ as per (3.5) (solid black arrow). Mean entrainment and local turbulence set the streamwise velocity jump according to (4.1). Viscous influence at the TNTI boundary determines δ_ω (dashed line, green online). Turbulent motions within the superlayer scale according to δ_ω and $D[U_t]$ (dash-dotted arrows, blue online). (*b*) Schematic representation of the observed scaling. Relative arrow sizes denoting δ_ω, $\mathcal{D}[\tilde{U}]$ and $\langle \tilde{W}_i \rangle$ are not to scale.

In a zero-pressure-gradient turbulent boundary layer the depth of viscous sublayer is approximately $5\,\nu/u_\tau$, while $\delta_\omega^+ \to$ constant at high Reynolds numbers. The similarities between the sublayer and the superlayer are not limited to their widths. The mean velocity in the viscous sublayer scales with u_τ while in the superlayer the velocity deficit scales with u_τ. However, the scalings of the viscous superlayer and of the viscous sublayer are independent, i.e. the presence of viscous sublayer does not

influence the scaling of the viscous superlayer. The scaling of viscous superlayer is due to the imposed skin-friction velocity u_τ, and is likely to hold even in the case of rough-wall boundary layers where the viscous sublayer ceases to exist accompanied by the form drag due to the roughness elements. The scaling by u_τ is explained by Townsend's outer similarity hypothesis and existence of this similarity is essential in our understanding.

As the flow develops downstream, the velocity jump at the interface $\mathcal{D}[\langle \tilde{U} \rangle]$ decreases with decreasing u_τ. This decrease is coincidental with the decrease in the average wall-normal velocity $\langle \tilde{W}_i \rangle$. Spatially the superlayer width increases with downstream distance in a developing boundary layer at a rate dictated by ν/u_τ (figure 10b). Since $\mathrm{d}\delta/\mathrm{d}x$ is much larger than $\mathrm{d}(\nu/u_\tau)/\mathrm{d}x$, the superlayer width relative to the boundary-layer depth asymptotes to zero (3.20).

An idealised superlayer jump profile and its statistical distribution of location results in a smeared profile that matches the mean velocity description. The dynamical similarity between the superlayer and the free-shear wake is explored here to partially explain the emergence of the 'wake' profile in the intermittent region. This physical phenomenon describes the presence of the wake profile with quantitative agreement in contrast to the purely empirical descriptions available in the literature for the wake profile.

Acknowledgements

Appendix A. A note on the three-dimensionality of TNTI (main analysis contributed by a reviewer)

Consider the TNTI as a two-dimensional surface bounding all turbulent flow below. Instantaneous interface height is represented as $\tilde{Z}_i = Z_i(x) + z_i'(x, y, t)$, where Z_i is the mean interface height and z_i' is the fluctuating height. Here we consider the $z_i'(x, y, t)$ as a single-valued function, i.e. in the regions where the interface folds back onto itself $\tilde{Z}_i$ is the upper envelope of the turbulent/non-turbulent boundary. The velocity of this interface is defined as $\boldsymbol{v}_I = (\tilde{U}_I, \tilde{W}_I, \tilde{V}_I) = (U_I + u_I', W_I + w_I', V_I + v_I')$ in the (x, z, y) directions, respectively. (Note that subscript 'I' is used to denote velocity of the interface and should not be confused with subscript 'i' used in the manuscript to denote a quantity at the interface.) The following properties are also noted:

(a) $\langle u_I' \rangle = \langle w_I' \rangle = \langle v_I' \rangle = 0$;
(b) $U_I \neq 0$ (the interface convects in the flow-direction);
(c) $W_I \neq 0$ (the mean interface height increases with down-stream distance);
(d) $V_I = 0$ (two-dimensional mean flow).

The rate of change of $\tilde{Z}_i = Z_i(x) + z_i'(x, y, t)$ in the Eulerian frame is equivalent to the interface velocity in z direction and can be written as

$$\tilde{W}_I = \frac{\partial \tilde{Z}_i}{\partial t} + \tilde{U}_I \frac{\partial \tilde{Z}_i}{\partial x} + \tilde{V}_I \frac{\partial \tilde{Z}_i}{\partial y}. \tag{A 1}$$

Splitting into mean and fluctuating components

$$W_I + w_I' = \frac{\partial z_i'}{\partial t} + (U_I + u_I') \frac{\partial (Z_i + z_i')}{\partial x} + v_I' \frac{\partial z_i'}{\partial y}. \tag{A 2}$$

Substituting $W_I = U_I \cdot (dZ_i/dx)$ gives

$$w_I' = \frac{\partial z_i'}{\partial t} + U_I \frac{\partial z_i'}{\partial x} + u_I' \frac{\partial (Z_i + z_i')}{\partial x} + v_I' \frac{\partial z_i'}{\partial y}. \tag{A 3}$$

An average of (A 3) then yields

$$\left\langle u_I' \frac{\partial z_i'}{\partial x} \right\rangle = - \left\langle v_I' \frac{\partial z_i'}{\partial y} \right\rangle. \tag{A 4}$$

Time-resolved measurements are needed to determine the displacement of TNTI over a small time interval Δt and thereby evaluate u_I'. Unfortunately, time-resolved information is not available to us from the present data and therefore left-hand side of (A 4) cannot be estimated accurately in our study. Two possibilities emerge for (A 4). First, u_I' and $\partial z_i'/\partial x$ are uncorrelated. In this case both terms in (A 4) are identically zero. Recently Wolf *et al.* (2013) demonstrated that turbulent fluctuations display a strong dependence on the local TNTI shape and that different entrainment mechanisms are dominant depending on the surface shape. Based on this evidence it is reasonable to assume that (A 4) holds a finite magnitude, i.e. u_I' and $\partial z_i'/\partial x$ are correlated. Furthermore, in two dimensions, $z_i'(x, t)$ detected in the streamwise/wall-normal plane has a fractal characteristic similar to $z_i'(y, t)$ detected in the spanwise/wall-normal plane. Therefore, $z_i'(x, t)$ and $z_i'(y, t)$ are statistically similar in geometry (Paizis & Schwarz 1974) and (A 4) indicates that $v_I' = O(u_I')$.

Now the interface velocity is related to the entrainment velocity and fluid velocity as

$$\boldsymbol{v}_I = \boldsymbol{v}_E + \boldsymbol{v}, \tag{A 5}$$

where the entrainment velocity $\boldsymbol{v}_E = (U_E + u_E', W_E + w_E', v_E')$ and the fluid velocity $\boldsymbol{v} = (U + u, W + w, v)$. Therefore

$$u_I' + U_I = u_E' + U_E + u + U \Rightarrow u_I' = u_E' + u. \tag{A 6}$$

We know that $u_E' = O(u_\tau)$ (Philip *et al.* 2014) and $u = O(u_\tau)$ from figure 8 of the present manuscript. Hence $u_I' = O(u_\tau)$. From (A 4) it can then be deduced that $v_I' = O(u_\tau)$. Hence, the fluctuating spanwise interface velocity also scales with u_τ.

REFERENCES

ADRIAN, R. J. 2007 Hairpin vortex organization in wall turbulence. *Phys. Fluids* **19**, 041301.

ADRIAN, R. J., MEINHART, C. D. & TOMKINS, C. D. 2000 Vortex organization in the outer region of the turbulent boundary layer. *J. Fluid Mech.* **422**, 1–54.

ANAND, R., BOERSMA, B. J. & AGRAWAL, A. 2009 Detection of turbulent/non-turbulent interface for an axisymmetric turbulent jet: evaluation of known criteria and proposal of a new criterion. *Exp. Fluids* **47** (6), 995–1007.

BERNARDINI, M., PIROZZOLI, S. & ORLANDI, P. 2014 Velocity statistics in turbulent channel flow up to $Re_\tau = 4000$. *J. Fluid Mech.* **742**, 171–191.

BISSET, D. K., HUNT, J. C. R. & ROGERS, M. M. 2002 The turbulent/non-turbulent interface bounding a far wake. *J. Fluid Mech.* **451**, 383–410.

BROWN, G. L. & ROSHKO, A. 1974 On density effects and large structure in turbulent mixing layers. *J. Fluid Mech.* **64**, 775–816.

CHAUHAN, K. A., MONKEWITZ, P. A. & NAGIB, H. M. 2009 Criteria for assessing experiments in zero pressure gradient boundary layers. *Fluid Dyn. Res.* **41**, 021404.

CHAUHAN, K., PHILIP, J., DE SILVA, C., HUTCHINS, N. & MARUSIC, I. 2014 The turbulent/non-turbulent interface and entrainment in a boundary layer. *J. Fluid Mech.* **742**, 119–151.

CHRISTENSEN, K. T. 2004 The influence of peak-locking errors on turbulence statistics computed from PIV ensembles. *Exp. Fluids* **36** (3), 484–497.

COLES, D. E. & HIRST, E. A. 1968 Computation of turbulent boundary layers. In *Proceedings of AFOSR-IFP Stanford Conference, Stanford, CA*, vol. 2.

CORRSIN, S. & KISTLER, A. L. 1955 Free-stream boundaries of turbulent flows. *NACA Tech. Rep.* TN-1244, Washington, DC.

DIMOTAKIS, P. E. 2005 Turbulent mixing. *Annu. Rev. Fluid Mech.* **37**, 329–356.

FALCO, R. E. 1977 Coherent motions in the outer region of turbulent boundary layers. *Phys. Fluids Suppl.* **20**, S132.

HAMBLETON, W., HUTCHINS, N. & MARUSIC, I. 2005 Simultaneous orthogonal plane PIV measurements in a turbulent boundary layer. *J. Fluid Mech.* **560**, 53–64.

HEAD, M. R. & BANDYOPADHYAY, P. 1981 New aspects of turbulent boundary-layer structure. *J. Fluid Mech.* **107**, 297–338.

HERPIN, S., STANISLAS, M., FOUCAUT, J. M. & COUDERT, S. 2013 Influence of the Reynolds number on the vortical structures in the logarithmic region of turbulent boundary layers. *J. Fluid Mech.* **716**, 5–50.

HOLZNER, M., LIBERZON, A., NIKITIN, N., KINZELBACH, W. & TSINOBER, A. 2007 Small-scale aspects of flows in proximity of the turbulent/nonturbulent interface. *Phys. Fluids* **19**, 071702.

HOLZNER, M., LIBERZON, A., NIKITIN, N., LÜTHI, B., KINZELBACH, W. & TSINOBER, A. 2008 A Lagrangian investigation of the small-scale features of turbulent entrainment through particle tracking and direct numerical simulation. *J. Fluid Mech.* **598**, 465–475.

HOLZNER, M. & LÜTHI, B. 2011 Laminar superlayer at the turbulence boundary. *Phys. Rev. Lett.* **106**, 134503.

HOYAS, S. & JIMÉNEZ, J. 2006 Scaling of the velocity fluctuations in turbulent channels up to $Re = 2003$. *Phys. Fluids* **18**, 011702.

HUFFMAN, D. G. & BRADSHAW, P. 1972 A note on von Kármán's constant in low Reynolds number turbulent flows. *J. Fluid Mech.* **53** (1), 45–60.

HUNT, J. C. R., ROTTMAN, J. W. & BRITTER, R. E. 1984 Some physical processes involved in the dispersion of dense gases. In *Proceedings of IUTAM Symposium 'Atmospheric Dispersion of Heavy Gases and Small Particles'* (ed. G. Ooms & H. Tennekes), pp. 361–395. Springer.

HUTCHINS, N. & MARUSIC, I. 2007 Evidence of very long meandering features in the logarithmic region of turbulent boundary layers. *J. Fluid Mech.* **579**, 1–28.

HUTCHINS, N., NICKELS, T. B., MARUSIC, I. & CHONG, M. S. 2009 Hot-wire spatial resolution issues in wall-bounded turbulence. *J. Fluid Mech.* **635**, 103–136.

JIMÉNEZ, J. & HOYAS, S. 2008 Turbulent fluctuations above the buffer layer of wall-bounded flows. *J. Fluid Mech.* **611**, 215–236.

KOVASZNAY, L. S. G. 1967 Structure of the turbulent boundary layer. *Phys. Fluids Suppl.* **10**, S25–S30.

KULANDAIVELU, V. 2012 Evolution of zero pressure gradient turbulent boundary layers from different initial conditions. PhD thesis, The University of Melbourne, Melbourne, Australia.

MARUSIC, I. & ADRIAN, R. J. 2012 The eddies and scales of wall turbulence. In *Ten Chapters in Turbulence* (ed. Y. Kaneda, K. R. Sreenivasan & P. A. Davidson), pp. 176–220. Cambridge University Press.

MARUSIC, I., UDDIN, A. K. M. & PERRY, A. E. 1997 Similarity law for the streamwise turbulence intensity in zero-pressure-gradient turbulent boundary layers. *Phys. Fluids* **9**, 3718–3726.

MEINHART, C. D. & ADRIAN, R. J. 1995 On the existence of uniform momentum zones in a turbulent boundary layer. *Phys. Fluids* **7**, 694–696.

MONKEWITZ, P. A., CHAUHAN, K. A. & NAGIB, H. M. 2007 Self-consistent high-Reynolds-number asymptotics for zero-pressure-gradient turbulent boundary layers. *Phys. Fluids* **19**, 115101.

MONKEWITZ, P. A., CHAUHAN, K. A. & NAGIB, H. M. 2008 Comparison of mean flow similarity laws in zero pressure gradient turbulent boundary layers. *Phys. Fluids* **20**, 105102.

MORRILL-WINTER, C. & KLEWICKI, J. 2013 Influences of boundary layer scale separation on the vorticity transport contribution to turbulent inertia. *Phys. Fluids* **25**, 015108.

MORTON, B. R., TAYLOR, G. I. & TURNER, J. S. 1956 Turbulent gravitational convection from maintained and instantaneous sources. *Phil. Trans. R. Soc. Lond.* A **234** (1196), 1–23.

MURLIS, J., TSAI, H. M. & BRADSHAW, P. 1982 The structure of turbulent boundary layers at low Reynolds numbers. *J. Fluid Mech.* **122** (1), 13–56.

NAGIB, H. M. & CHAUHAN, K. A. 2008 Variations of von Kármán coefficient in canonical flows. *Phys. Fluids* **20**, 101518.

NEE, V. W. & KOVASZNAY, L. S. G. 1969 Simple phenomenological theory of turbulent shear flows. *Phys. Fluids* **12**, 473.

PAIZIS, S. T. & SCHWARZ, W. H. 1974 An investigation of the topography and motion of the turbulent interface. *J. Fluid Mech.* **63** (2), 315–343.

PHILIP, J. & MARUSIC, I. 2012 Large-scale eddies and their role in entrainment in turbulent jets and wakes. *Phys. Fluids* **24**, 055108.

PHILIP, J., MENEVEAU, C., DE SILVA, C. M. & MARUSIC, I. 2014 Multiscale analysis of fluxes at the turbulent/non-turbulent interface in high Reynolds number boundary layers. *Phys. Fluids* **26** (1), 015105.

POPE, S. B. 2000 *Turbulent Flows*. Cambridge University Press.

REYNOLDS, W. C. 1972 Large-scale instabilities of turbulent wakes. *J. Fluid Mech.* **54**, 481–488.

SCHULTZ, M. P. & FLACK, K. A. 2007 The rough-wall turbulent boundary layer from the hydraulically smooth to the fully rough regime. *J. Fluid Mech.* **580**, 381–405.

DA SILVA, C. B. & DOS REIS, R. J. N. 2011 The role of coherent vortices near the turbulent/non-turbulent interface in a planar jet. *Phil. Trans. R. Soc. Lond.* A **369**, 738–753.

DA SILVA, C. B., HUNT, J. C. R., EAMES, I. & WESTERWEEL, J. 2014 Interfacial layers between regions of different turbulence intensity. *Annu. Rev. Fluid Mech.* **46** (1), 567–590.

DA SILVA, C. B. & PEREIRA, J. C. F. 2008 Invariants of the velocity-gradient, rate-of-strain, and rate-of-rotation tensors across the turbulent/nonturbulent interface in jets. *Phys. Fluids* **20** (5), 055101.

DA SILVA, C. B. & TAVEIRA, R. R. 2010 The thickness of the turbulent/nonturbulent interface is equal to the radius of the large vorticity structures near the edge of the shear layer. *Phys. Fluids* **22**, 121702.

DA SILVA, C. B. & TAVEIRA, R. R. 2013 The turbulent/non-turbulent interface and viscous superlayer in turbulent planar jets. In *Proceedings of 14th European Turbulence Conference, 1–4 September, Lyon, France*.

DE SILVA, C. M., CHAUHAN, K. A., ATKINSON, C. H., BUCHMANN, N. A., HUTCHINS, N., SORIA, J. & MARUSIC, I. 2012 Implementation of large scale PIV measurements for wall bounded turbulence at high Reynolds numbers. In *Proceedings of 18th Australasian Fluid Mechanics Conference, 3–7 December, Launceston, Australia*.

DE SILVA, C. M., GNANAMANICKAM, E. P., ATKINSON, C., BUCHMANN, N. A., HUTCHINS, N., SORIA, J. & MARUSIC, I. 2014 High spatial range velocity measurements in a high Reynolds number turbulent boundary layer. *Phys. Fluids* **26** (2), 025117.

DE SILVA, C. M., PHILIP, J., CHAUHAN, K., MENEVEAU, C. & MARUSIC, I. 2013 Multiscale geometry and scaling of the turbulent-nonturbulent interface in high Reynolds number boundary layers. *Phys. Rev. Lett.* **111**, 044501.

SMITS, A. J., MCKEON, B. J. & MARUSIC, I. 2011 High-Reynolds number wall turbulence. *Annu. Rev. Fluid Mech.* **43**, 353–375.

SREENIVASAN, K. R., PRASAD, R. R., MENEVEAU, C. & RAMSHANKAR, R. 1989*a* The fractal geometry of interfaces and the multifractal distribution of dissipation in fully turbulent flows. *Pure Appl. Geophys.* **131** (1), 43–60.

SREENIVASAN, K. R., RAMSHANKAR, R. & MENEVEAU, C. 1989*b* Mixing, entrainment and fractal dimensions of surfaces in turbulent flows. *Phil. Trans. R. Soc. Lond.* A **421** (1860), 79–108.

TAVEIRA, R. R. & DA SILVA, C. B. 2013 Kinetic energy budgets near the turbulent/nonturbulent interface in jets. *Phys. Fluids* **25**, 015114.

TAYLOR, G. I. 1938 Production and dissipation of vorticity in a turbulent fluid. *Phil. Trans. R. Soc. Lond.* A **164** (916), 15–23.

TENNEKES, H. & LUMLEY, J. L. 1972 *A First Course in Turbulence*. The MIT Press.

TOWNSEND, A. A. 1956 *The Structure of Turbulent Shear Flow*, 1st edn. Cambridge University Press.

TOWNSEND, A. A. 1976 *The Structure of Turbulent Shear Flow*, 2nd edn. Cambridge University Press.

TURNER, J. S. 1986 Turbulent entrainment: the development of the entrainment assumption, and its application to geophysical flows. *J. Fluid Mech.* **173**, 431–471.

WESTERWEEL, J., FUKUSHIMA, C., PEDERSEN, J. M. & HUNT, J. C. R. 2005 Mechanics of the turbulent-nonturbulent interface of a jet. *Phys. Rev. Lett.* **95**, 174501.

WOLF, M., HOLZNER, M., LÜTHI, B., KRUG, D., KINZELBACH, W. & TSINOBER, A. 2013 Effects of mean shear on the local turbulent entrainment process. *J. Fluid Mech.* **731**, 95–116.

WOLF, M., LÜTHI, B., HOLZNER, M., KRUG, D., KINZELBACH, W. & TSINOBER, A. 2012 Investigations on the local entrainment velocity in a turbulent jet. *Phys. Fluids* **24**, 105110.

WU, Y. & CHRISTENSEN, K. T. 2007 Outer-layer similarity in the presence of a practical rough-wall topography. *Phys. Fluids* **19**, 085108.